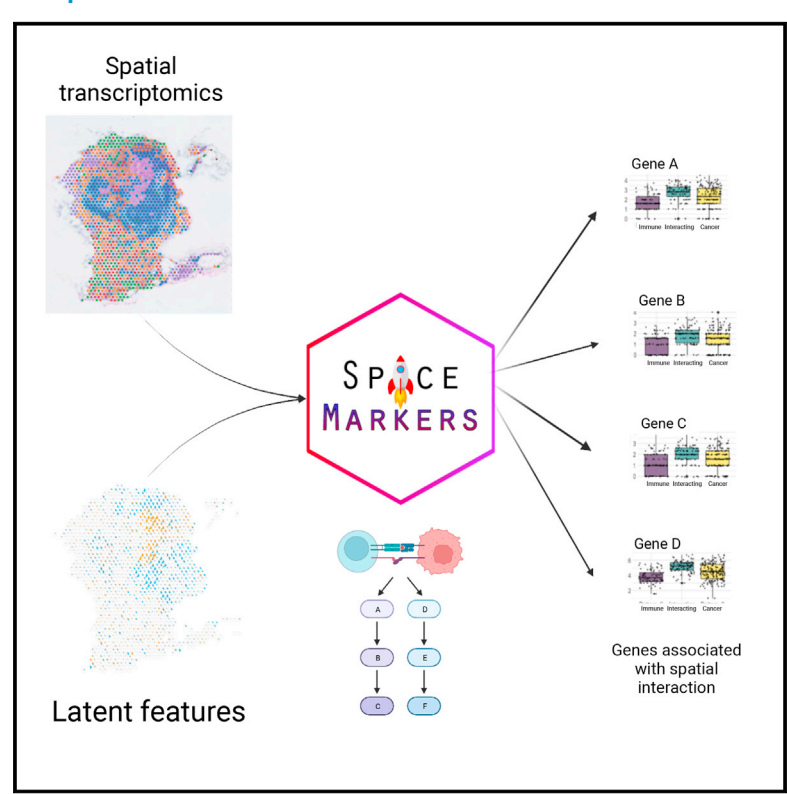
Uncovering the spatial landscape of molecular interactions within the tumor microenvironment through latent spaces

Graphical abstract



Authors

Atul Deshpande, Melanie Loth, Dimitrios N. Sidiropoulos, ..., Genevieve Stein-O'Brien, Luciane T. Kagohara, Elana J. Fertig

Correspondence

ejfertig@jhmi.edu

In brief

Deshpande, Loth, et al. present
SpaceMarkers as an algorithm to identify
molecular changes resulting from cell-cell
interactions using latent space analysis of
spatial transcriptomics. SpaceMarkers
uses spatial co-localization of latent
features as direct evidence of cellular
interactions and applies the method to
analyze the tumor-immune interactions
across tumor types.

Highlights

- Latent space analyses of spatial transcriptomics show spatially varying cellular activity
- SpaceMarkers identifies genes associated with spatially interacting latent features
- SpaceMarkers identifies molecular changes from tumorimmune interactions in various tumors







Methods

Uncovering the spatial landscape of molecular interactions within the tumor microenvironment through latent spaces

Atul Deshpande, 1,2,3,13 Melanie Loth, 1,2,3,13 Dimitrios N. Sidiropoulos, 1,2,3,4 Shuming Zhang,5 Long Yuan,3,6 Alexander T.F. Bell,1,2,3 Qingfeng Zhu,1,2,3 Won Jin Ho,1,2,3 Cesar Santa-Maria,1 Daniele M. Gilkes,1 Stephen R. Williams,7 Cedric R. Uytingco,7 Jennifer Chew,7 Andrej Hartnett,7 Zachary W. Bent,7 Alexander V. Favorov,1,2,3 Aleksander S. Popel,1,5 Mark Yarchoan,1,2,3 Ashley Kiemen,1,8 Pei-Hsun Wu,9 Kohei Fujikura,8 Denis Wirtz,1,2,3,8,9,10 Laura D. Wood,1,8,11 Lei Zheng,1,2,3 Elizabeth M. Jaffee,1,2,3 Robert A. Anders,2,3,8 Ludmila Danilova,1,2,3 Genevieve Stein-O'Brien,1,2,3 Luciane T. Kagohara,1,2,3 and Elana J. Fertig1,2,3,5,12,14,*

SUMMARY

Recent advances in spatial transcriptomics (STs) enable gene expression measurements from a tissue sample while retaining its spatial context. This technology enables unprecedented *in situ* resolution of the regulatory pathways that underlie the heterogeneity in the tumor as well as the tumor microenvironment (TME). The direct characterization of cellular co-localization with spatial technologies facilities quantification of the molecular changes resulting from direct cell-cell interaction, as it occurs in tumor-immune interactions. We present SpaceMarkers, a bioinformatics algorithm to infer molecular changes from cell-cell interactions from latent space analysis of ST data. We apply this approach to infer the molecular changes from tumor-immune interactions in Visium spatial transcriptomics data of metastasis, invasive and precursor lesions, and immunotherapy treatment. Further transfer learning in matched scRNA-seq data enabled further quantification of the specific cell types in which SpaceMarkers are enriched. Altogether, SpaceMarkers can identify the location and context-specific molecular interactions within the TME from ST data.

INTRODUCTION

The tumor microenvironment (TME) is the tissue region created and controlled by a tumor in its surroundings and plays a key role in tumorigenesis and therapeutic response in cancer. ^{1–4} The TME contains tumor cells, stroma, blood vessels, and immune cells as well as cells from the resident tissue. ⁴ A thorough understanding of the molecular profile of individual cells and the impact of intercellular interactions in the TME is crucial for distinguishing the determinants of tumor progression ^{5–7} and precision medicine strategies. ^{3,8–11}

Advances in single-cell technologies have led to the development of spatially resolved transcriptomics (STs) that captures the transcriptome $in \ situ^{12}$ and thus allows us to study the spatial relationship between the various cell populations within the TME and their relationship with the tumor cells. For example, the 10X Visium spatial transcriptomic technology allows us to resolve tissue heterogeneity at a near single-cell resolution (from one to tens of cells per spot). The technique has been applied to characterize the cellular and molecular compositions of tumors. $^{13-15}$ Robust analysis pipelines for cell-based analysis and cellular deconvolution have been proposed to model the



¹Department of Oncology, Sidney Kimmel Comprehensive Cancer Center, Johns Hopkins University School of Medicine, Baltimore, MD, USA ²Convergence Institute, Johns Hopkins University, Baltimore, MD, USA

³Bloomberg-Kimmel Institute for Cancer Immunotherapy, Johns Hopkins University School of Medicine, Baltimore, MD, USA

⁴Cellular and Molecular Medicine, Johns Hopkins University School of Medicine, Baltimore, MD, USA

⁵Department of Biomedical Engineering, Johns Hopkins University School of Medicine, Baltimore, MD, USA

⁶Department of Immunology, Johns Hopkins University School of Medicine, Baltimore, MD, USA

⁷10x Genomics, Inc., Pleasanton, CA, USA

⁸Department of Pathology, Johns Hopkins University School of Medicine, Baltimore, MD, USA

⁹Department of Chemical and Biomolecular Engineering, Johns Hopkins University Whiting School of Engineering, Baltimore, MD, USA

¹⁰Johns Hopkins Physical Sciences - Oncology Center and Institute for NanoBioTechnology, Johns Hopkins University, Baltimore, MD, USA

¹¹The Sol Goldman Pancreatic Cancer Research Center, Johns Hopkins University School of Medicine, Baltimore, MD, USA

¹²Department of Applied Mathematics and Statistics, Johns Hopkins University Whiting School of Engineering, Baltimore, MD, USA

¹³These authors contributed equally

¹⁴Lead contact

^{*}Correspondence: ejfertig@jhmi.edu https://doi.org/10.1016/j.cels.2023.03.004





cellular composition of spatial-transcriptomics data^{16–20} and cellular phenotypes within each spot.²¹ Although spot deconvolution methods can infer linear combinations of molecular markers that are reflective of cellular co-localization, new computational methods are needed to characterize the molecular changes resulting from cell-cell interactions at a genome-wide scale.

Many analysis pipelines for Visium ST rely on the latent space methods for cellular deconvolution to overcome the mixture of cells at each spot. In this paper, we present the SpaceMarkers algorithm that leverages spatially interacting latent features to infer molecular changes resulting from interactions between cell types or biological processes represented by the features. SpaceMarkers uses a kernel-based smoothing approach to model the influence of a highly expressed feature in a spot extending to its neighboring spots as well. Using latent features inferred from CoGAPS,²² we demonstrate the broad utility of SpaceMarkers to infer molecular changes resulting from cellcell interactions in Visium samples from invasion to lymph node, pancreatic premalignant lesions, breast primary tumor, and immunotherapy-treated cancer. We selected CoGAPS, a Bayesian nonnegative matrix factorization approach, based on its robustness for single-cell RNA-seq data.^{23,24} We also show the compatibility of SpaceMarkers with other latent space methods, using STdeconvolve¹⁷ as an example. Further extension of this approach to integrate Visium data with single-cell data through transfer learning also enables the identification of the precise cell subtypes in which the molecular changes from cell-cell interactions are introduced. Altogether, our extension to the latent space analysis enables us to simultaneously infer cellular architecture and model molecular changes resulting from spatially interacting biological processes.

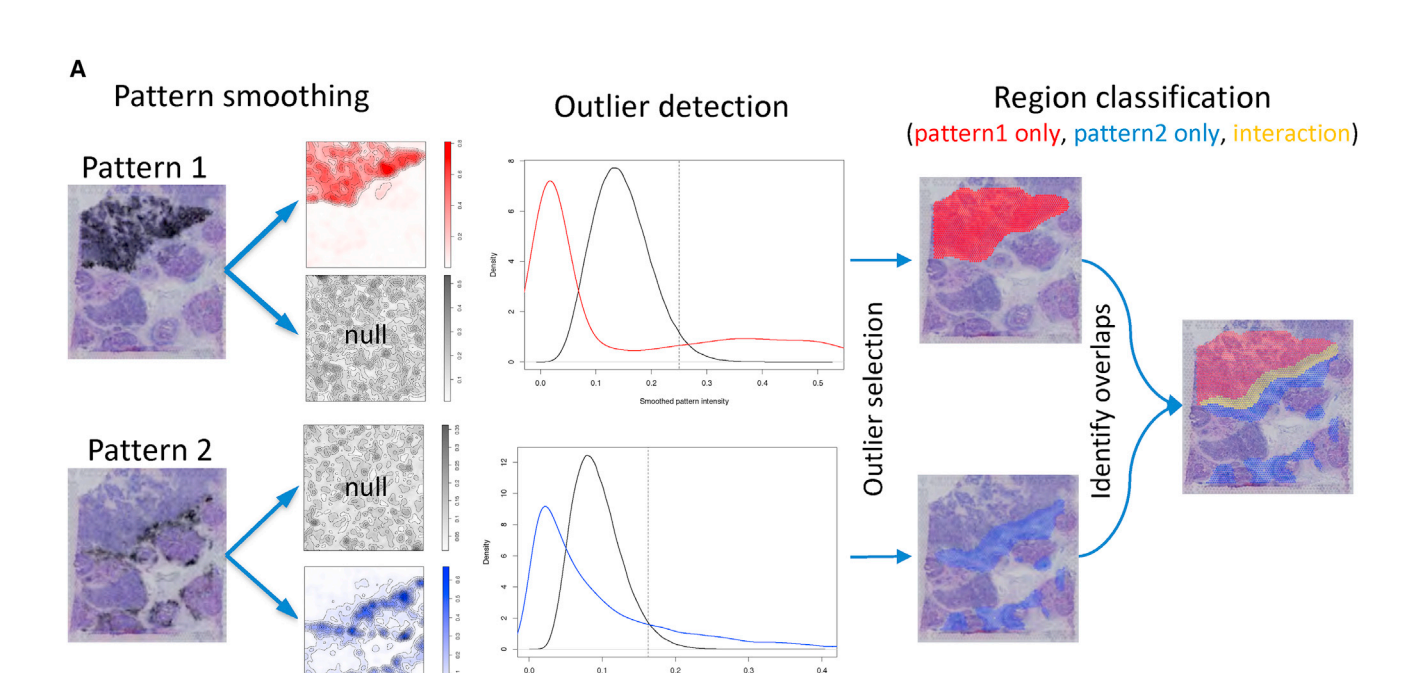
RESULTS

Interactions between overlapping latent features delineate intercellular interactions in ST data

Here, we present SpaceMarkers, a bioinformatics algorithm for identifying genes associated with cell-cell interactions in ST data. SpaceMarkers is an extension of the latent space analysis that leverages spatially overlapping latent features associated with distinct cellular signatures to infer the genes associated with their interaction (Figure 1). Fundamentally, this inference relies on the estimation of spatially resolved latent features representative of cellular signatures in the ST data. That is, the latent feature information is characterized by continuous weights corresponding to each spatial coordinate in the ST data. We denote these continuous weights as the patterns in the ST data. The inputs to the SpaceMarkers algorithm are the ST data matrix and spatially resolved patterns learned through the latent space analysis, and the output is a list of genes associated with the interaction between each pair of spatially overlapping patterns. The first stage of the algorithm involves the identification of each pattern's region of influence and subsequently the region of pattern interaction (Figure 1A; see also STAR Methods). If a pattern has a nonzero value at a point, we hypothesize that its influence extends to its neighboring region but rapidly decreases with increasing distance. We model this by spatially smoothing the patterns using a Gaussian kernel-based approach (see STAR

Methods). Subsequently, we identify the outlier values of smoothed patterns by testing them against a null distribution obtained by the identical smoothing of spatially permuted pattern values. We denote the region corresponding to these outlier values as the region of influence of the pattern. Furthermore, two patterns are deemed to be interacting in the region with overlapping influence from both patterns. We hypothesize that genes associated with the spatially overlapping influence from two patterns represent changes in the molecular pathways due to the interaction between the biological features of the associated cells. Therefore, we devise the second stage of the SpaceMarkers algorithm to rank genes exhibiting higher activity levels in the interaction region relative to regions with exclusive influence from each pattern (Figure 1B; see also STAR Methods). To this end, we perform a non-parametric statistical test followed by the post-hoc analysis to identify these genes that constitute the SpaceMarkers output.

In the examples demonstrated here, the spatial data are obtained using the spot-based 10x Visium spatial transcriptomics technology¹² with 1-10 cells per spot. SpaceMarkers is readily applicable to spot-based ST data with regions of influence and interaction defined as sets of spots in which one or two patterns, respectively, have influence as identified by the Gaussian kernelbased approach. We use CoGAPS Bayesian nonnegative matrix factorization^{22,25} for identifying the latent features associated with cellular signatures. When two patterns have overlapping influences in the same region of the tissue, we assume an interaction between these patterns in this interaction region. We provide a differential expression (DE) mode for SpaceMarkers to quantify genes with enhanced expressions in a region with overlapping influence from two patterns when compared with regions with exclusive influence from individual patterns. This DE mode allows for broad applicability across latent space methods, which we demonstrate by applications using CoGAPS and STDeconvolve.¹⁷ Furthermore, we extend this approach to provide a "residual" mode—which identifies genes that have significantly higher residual error between the original ST data and its estimated fit from the CoGAPS model in the region with overlapping influence from two patterns when compared with the regions with exclusive influence from each pattern. We hypothesize that the residual mode detects the nonlinear effects of intercellular interaction more precisely by accounting for the underlying linear latent features to mitigate confounding effects from variations in the cell population density and cell types with common markers. Thus, the SpaceMarkers algorithm infers both simple molecular changes in the "DE" mode and more precise nonlinear molecular changes in the residual mode in regions with overlapping influence from patterns associated with different cell signatures. We denote such patterns with concurrent influence in a region as "spatially interacting" patterns. The reliance on latent space patterns from CoGAPS enables the further ability to integrate SpaceMarkers learned from ST data in corresponding single-cell data using transfer learning from projectR^{24,26} to refine the specific cells in which these molecular changes occur. Although the examples in this paper use latent space patterns in ST data from CoGAPS or STdeconvolve to define cellular signatures, it is generally applicable to the output of any of a number of latent feature factorization approaches available in the literature.



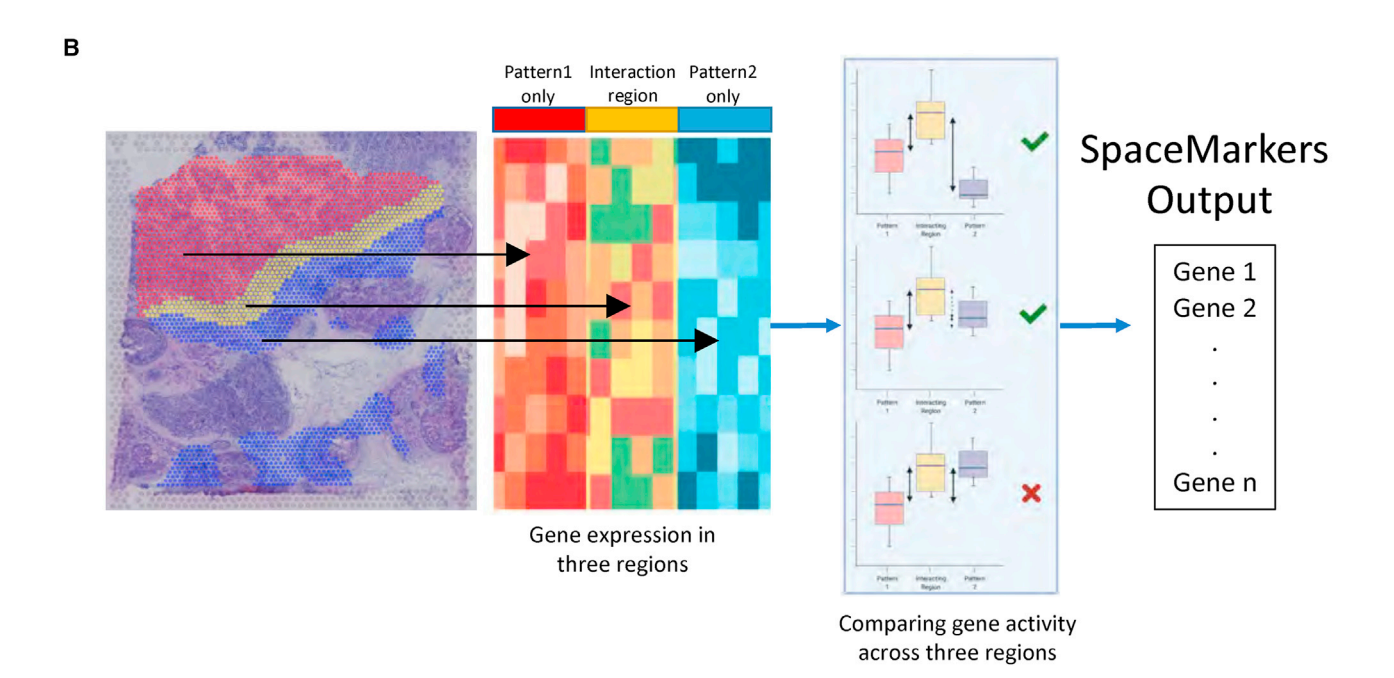


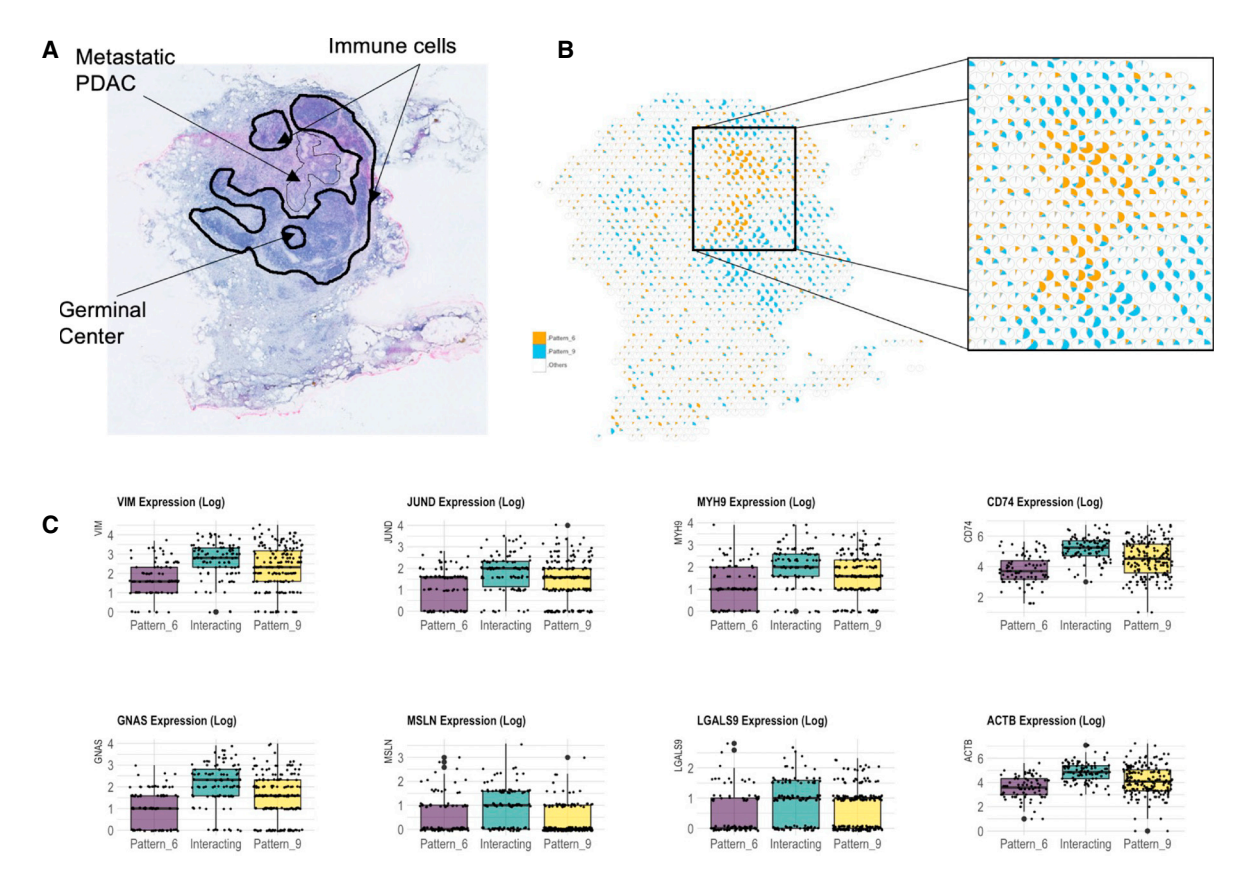
Figure 1. SpaceMarkers identifies genes associated with cell-cell interactions using spatially overlapping patterns

(A) Identifying the interaction region: the input to the SpaceMarkers algorithm are spatially resolved latent features resulting from latent space analyses (e.g., CoGAPS patterns). The images on the left show the intensity levels of two spatially resolved CoGAPS patterns. For each pattern, the SpaceMarkers algorithm first identifies regions of influence (red and blue spots, respectively) using a Gaussian-kernel based outlier detection method. The patterns are deemed to be interacting in the region with overlapping influence (yellow spots) from both patterns. It also identifies regions with mutually exclusive influence from each pattern (red and blue spots).

(B) Identifying SpaceMarkers genes: the second stage of the SpaceMarkers algorithm performs a non-parametric Kruskal-Wallis statistical test with post-hoc analysis on the gene expression data in the three regions (pattern 1 only, pattern 2 only, and interaction region) to identify molecular changes due to cell-cell interaction. The output is a list of genes associated with the pattern interaction (see STAR Methods).







Gene Set Name	# Genes in Gene Set	# Genes in Overlap	p-value	FDR q-value
HALLMARK MYC TARGETS V1	200	39	5.34E-35	1.41E-32
HALLMARK ALLOGRAFT REJECTION	200	29	1.70E-22	1.80E-20
HALLMARK OXIDATIVE PHOSPHORYLATION	200	24	6.73E-17	3.55E-15
HALLMARK INTERFERON GAMMA RESPONSE	200	21	8.69E-14	2.70E-12
HALLMARK INTERFERON ALPHA RESPONSE	97	13	2.21E-10	4.87E-09
HALLMARK APICAL JUNCTION	200	16	4.40E-09	8.01E-08
HALLMARK MTORC1 SIGNALING	200	16	4.40E-09	8.01E-08
HALLMARK P53 PATHWAY	200	16	4.40E-09	8.01E-08
HALLMARK PI3K AKT MTOR SIGNALING	105	12	7.03E-09	1.16E-07
HALLMARK G2M CHECKPOINT	200	15	3.18E-08	4.94E-07
HALLMARK COMPLEMENT	200	14	2.14E-07	3.14E-06
HALLMARK APOPTOSIS	161	12	8.08E-07	1.09E-05
HALLMARK EPITHELIAL MESENCHYMAL TRANSITION	200	12	7.72E-06	9.26E-05
HALLMARK COAGULATION	138	10	8.55E-06	1.00E-04
HALLMARK UNFOLDED PROTEIN RESPONSE	113	9	1.13E-05	1.29E-04
HALLMARK INFLAMMATORY RESPONSE	200	11	4.09E-05	4.32E-04
HALLMARK GLYCOLYSIS	200	10	1.98E-04	1.94E-03
HALLMARK HYPOXIA	200	10	1.98E-04	1.94E-03
HALLMARK UV RESPONSE UP	158	8	7.82E-04	6.07E-03
HALLMARK MITOTIC SPINDLE	199	9	8.41E-04	6.30E-03
HALLMARK E2F TARGETS	200	9	8.71E-04	6.30E-03
HALLMARK MYOGENESIS	200	9	8.71E-04	6.30E-03
HALLMARK TNFA SIGNALING VIA NFKB	200	9	8.71E-04	6.30E-03
HALLMARK DNA REPAIR	150	7	2.61E-03	1.66E-02
HALLMARK IL2 STAT5 SIGNALING	199	8	3.34E-03	2.00E-02
HALLMARK ADIPOGENESIS	200	8	3.44E-03	2.04E-02
HALLMARK MYC TARGETS V2	58	4	5.62E-03	2.97E-02

(legend on next page)

Methods



SpaceMarkers identifies molecular changes from tumor-immune interactions associated with metastatic pancreatic cancer cells invading the lymph node

In the first example, we applied SpaceMarkers on Visium ST data from pancreatic cancer metastasis to the lymph node in a patient who received neoadjuvant GVAX vaccination (see Figure 2). More specifically, this sample is characterized by the presence of metastatic pancreatic ductal adenocarcinoma (PDAC), immune cell aggregates, and germinal centers of B cell maturation (Figure 2A). The analysis of H&E imaging from the lymph node region used to generate the ST data identifies a region of the tissue in which the metastatic PDAC intersects the immune cells surrounding the germinal center. On factorizing these data using CoGAPS, we obtain ten latent patterns based only on the expression data (Figure S1; STAR Methods). By matching pattern activity levels learned from the data with the independent histological annotations, we observe that CoGAPS can distinguish metastatic PDAC in pattern 6 from immune cells in the surrounding lymph node tissue in pattern 9 (Figure 2B).

We further analyzed the spatial activity of the metastatic PDAC (pattern 6) and immune (pattern 9) patterns to identify the regions of overlapping influence to associate with metastasis-immune interaction. We represent the spatial variation in the activity levels of pattern 6 and pattern 9 in relation to all the other patterns in each spot (Figure 2B). This proportional analysis of patterns enables us to observe a spatial overlap between the regions where pattern 6 and pattern 9 are active. However, we hypothesize that a pattern has an influence in a spot even with zero pattern activity but high-pattern activity levels in the neighboring spots. SpaceMarkers first identifies the region with spatially overlapping influence from these two patterns as their interaction region. Next, the SpaceMarkers algorithm identifies the gene expression changes that occur from metastasis-immune interaction in this interaction region (Data S1; Table S2). Due to the limited number of spots where the two patterns have overlapping influences, we define SpaceMarkers based on DEs. This analysis identifies 1,442 genes that exhibit a higher average expression in the interaction region with an overlapping influence from the two patterns compared with spots where only metastatic PDAC in pattern 6 or immune cells in pattern 9 have exclusive influence (see STAR Methods for details of the statistical test, Table S2 for the complete gene list with the associated statistics). The SpaceMarkers optParams values are tabulated in Table S1.

Figure S1 shows the expression heatmap of the Space Markers genes in spots belonging to regions with exclusive influence from the metastatic PDAC pattern 6, exclusive

influence from the immune cell pattern 9, and overlapping influence from both patterns in metastasis-immune interactions. In all cases, the interactions are associated with the changes in extracellular matrix genes, including notably genes associated with cytoskeleton regulation (TMSB10, TMSB4X, CFL1, and MARCKSL1), the myosin pathway (MYL6, MYH9, and MYL12B), actin regulation (ACTB, ACTN4, CAPG, LCP1, and SPTBN1), the matrix metallopeptidase family (MMP9 and MMP12), galectin genes (LGALS1, LGALS4, LGALS9, and LGALS3BP), collagen (COL1A2, COL3A1, COL4A1, COL4A2, COL18A1, and COL6A2), and cell adhesion (MSLN, ITGB4, ITGB6, and ADRM1). The SpaceMarkers include genes reflecting cell death in the increased expression of ribosomal protein genes associated with immune response through the expression of HLA family genes, immunogloblulins, interleukins, cytokines, chemokines, the interferon pathway IFITM2, and immune function. This immune response is counterbalanced by the changes to the pathways associated with enhanced invasion in cancer cells, including JUNB, JUND, and VIM.

To further elucidate the molecular pathways associated with the metastasis-immune interaction in the lymph node, we performed gene set overrepresentation analyses (Figure 2D; Table S2) from the Hallmark, KEGG, and Biocarta molecular pathways using the Molecular Signatures Database (MSigDB).²⁷⁻²⁹ As seen in Figure 2D, Hallmark pathways related to allograft rejection, interferon-gamma, and interferon-alpha are all overrepresented in the pathway analysis for the SpaceMarkers genes, and hence, in the region of overlap between the immune and metastatic PDAC patterns. This confirms the activation of the immune response for tumor rejection at the interface between the metastatic PDAC and the immune cells in the lymph node observed at the gene level. Likewise, we observe overrepresentation in the epithelial to mesenchymal signaling and pathways consistent with the invasive process in the metastatic PDAC cells, further supported by the enrichment of the apical junction consistent with the changes to the extracellular matrix suggested by the gene-level SpaceMarkers analysis.

The DE mode of SpaceMarkers is applicable when the available latent features provide only a partial reconstruction of the original ST data matrix. However, the DE of a marker in the interaction region could occur because of cell-cell interactions or confounders such as variable cell populations in each spot and different co-localized cell types having common markers. In the examples to follow, we mitigate these confounding effects by using the residual error between the raw expression and its reconstruction from the CoGAPS patterns, which capture the

Figure 2. SpaceMarkers identifies molecular changes associated with immune-metastatic pancreatic cancer interaction in the lymph node (A) H&E staining of a peritumoral pancreatic lymph node with metastasis from PDAC (arrow) and annotated germinal center and immune cells (dark lines).

⁽B) Visualization of the relative activity in the CoGAPS patterns associated with metastatic PDAC (pattern 6) and immune cells in the lymph node (pattern 9). Each spot is represented as a pie chart with fractional gene expression at the location aggregated over the all genes for pattern 6 (orange), pattern 9 (blue), and all other patterns put together (white).

⁽C) Boxplots of the expression of selected genes showing higher expression levels in the interaction region of pattern 6 and pattern 9 compared with the regions with exclusive influence from pattern 6 and pattern 9, respectively.

⁽D) Table showing Hallmark gene set pathways significantly overrepresented in the region of interaction between pattern 6 and pattern 9, with the size of overlap and FDR value (see Table S2 for KEGG and Biocarta pathways). See also Figure S1.



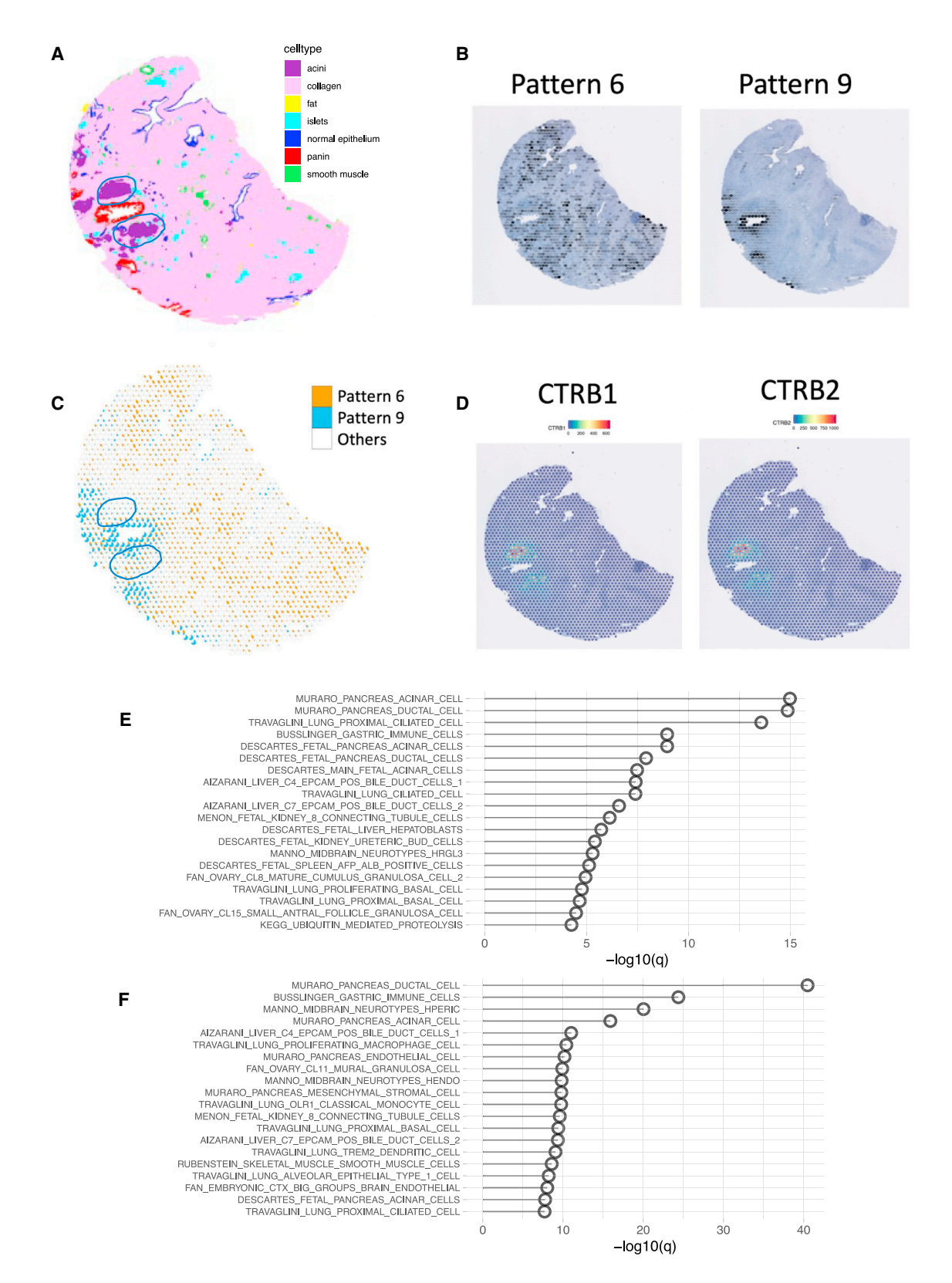


Figure 3. Residual mode can help to mitigate the confounding effects of other cell types present in the interaction region (A) Tissue regions annotated by CODA based on morphological features show clusters of acinar cells in close proximity to the neoplasia duct. (B) CoGAPS analysis reveals two patterns representing the stromal region (pattern 6, orange), the neoplasia region (pattern 9, blue), and all other patterns (white).



effect of both variations in cell population density as well as variations in individual marker expression.

Confounding factors from unrelated cell populations can be mitigated by using SpaceMarkers in residuals mode

Using SpaceMarkers in the DE mode identifies genes that are enriched relative to two patterns, but the output is susceptible to confounding factors from cell types independent of the two patterns of interest. For example, if the interaction region between two patterns contains an independent cell type that is not significantly present in the regions of exclusive influence of either pattern, we hypothesize that the cell-type-specific genes for the additional cell type will appear as space markers. To test this hypothesis, we applied SpaceMarkers to a sample of pancreatic intraepithelial neoplasia (PanIN),30 a premalignant lesion associated with PDAC (Figure 3). As described in our previous study of this sample, the H&E imaging provided with the Visium formalin-fixed paraffin-embedded (FFPE) technology used to profile this sample enabled us to determine cell types within the slide at a single-cell resolution using CODA,31 a deep-learning classifier that annotates tissue regions based on their morphological features (Figure 3A). This ground truth of cellular features also enables us to benchmark the latent space estimates of cellular features from CoGAPS. In this sample, we learned 10 transcriptional patterns from the PanIN using CoGAPS. Pattern 9 captures the PanIN on the tissue, and pattern 6 captures a majority of stromal cells (Figure 3B). The PanIN is surrounded by two large acini, which express high quantities of pancreatic enzymes that are not expressed elsewhere on the slide (Figure 3D). The interaction region between patterns 6 and 9 captures much of these acini. The SpaceMarkers analyses of these patterns in the DE mode results in several of the wellcharacterized pancreatic enzymes (Data S1) produced exclusively by acinar cells.³² Pathway analysis reveals that pancreatic acinar cell gene set is the most overrepresented gene set (Figure 3E; Table S3).

In the residuals mode, SpaceMarkers accounts for the gene signatures captured by CoGAPS patterns. Because pattern 5 represents the acinar cells in our dataset (Figure S2), we hypothesize that the residuals mode attenuates the confounding factor due to the acinar cells (Data S1). Unlike the DE mode, the top pathway for residuals mode is no longer a pancreatic acinar cell pathway (Figure 3F; Table S3). Residuals mode boosts the signal from pathways that are highly overrepresented in the DE mode, although maintaining the significance of the acinar gene sets. Collectively, these results show that genes captured by the DE mode can represent additional cell types that are not present in either patterns of interest. In addition, if these cell type signatures are unique and strong enough to be captured as an inde-

pendent transcriptional pattern, the residuals mode is capable of attenuating the signal from this additional cell type relative to other expression changes present in the interaction region. The SpaceMarkers optParams values are tabulated in Table S1.

SpaceMarkers identifies the markers of tumor-immune interactions in invasive breast ductal carcinoma through the residual space analysis

Although providing a means to detect molecular changes from cellular interactions in limited interaction regions, using DE statistics for SpaceMarkers could confound nonlinear effects from cell-cell interactions with expression changes resulting from the increased density of co-localized cell types with shared gene markers. In cases where the interaction region extends across a greater number of spots, these confounding effects can be mitigated by using the residual error between the raw expression and its estimated fit from the CoGAPS model for the SpaceMarkers. This estimated fit will capture the effect of both variations in cell population density and variations in individual marker expression to refine the estimates of the nonlinear effects from cell-cell interactions. We apply this approach to identify the molecular pathways associated with tumor cells and immune interactions in ST data from a breast cancer sample that contains multiple ductal carcinoma in situ (DCIS) lesions, an invasive carcinoma lesion, immune cells, and stroma (Figure 4A).

The visualization in Figure 4B shows widespread spatial regions of interactions between immune and tumor cells at the boundaries of both the invasive carcinoma and the DCIS lesions and some isolated spots of immune activity in the interior of the invasive tumor. However, the immune activity in these spots is not significantly over the threshold to create substantial immune influence in the neighborhood. Thus, the immune-invasive cancer interaction is largely contained near the boundary of the tumor. Although the pancreatic cancer sample in Figure 2 covered a smaller area with fewer spots (<300) having tumor and immune influences, respectively, we identify much larger regions (> 1000 spots) of influence from the immune, invasive carcinoma, and DCIS cells (Figure 4B). This larger number of spots enables us to estimate SpaceMarkers from CoGAPS residuals to distinguish the molecular changes in invasive carcinoma from the DCIS lesions. Similar to our analysis of the metastatic pancreatic cancer data, we obtain latent features of the ST data from this breast sample using CoGAPS factorization. These latent features reveal histological annotations of invasive carcinoma, DCIS lesions, immune, and stromal regions estimated from the H&E stain (Figure 4A).

Computing SpaceMarkers based on the CoGAPS residuals identifies 461 genes associated with interactions between the immune and invasive carcinoma patterns and 413 markers of immune and DCIS pattern interactions (Data S1), compared with up to 3,736 immune-invasive carcinoma and 3,036 immune-DCIS

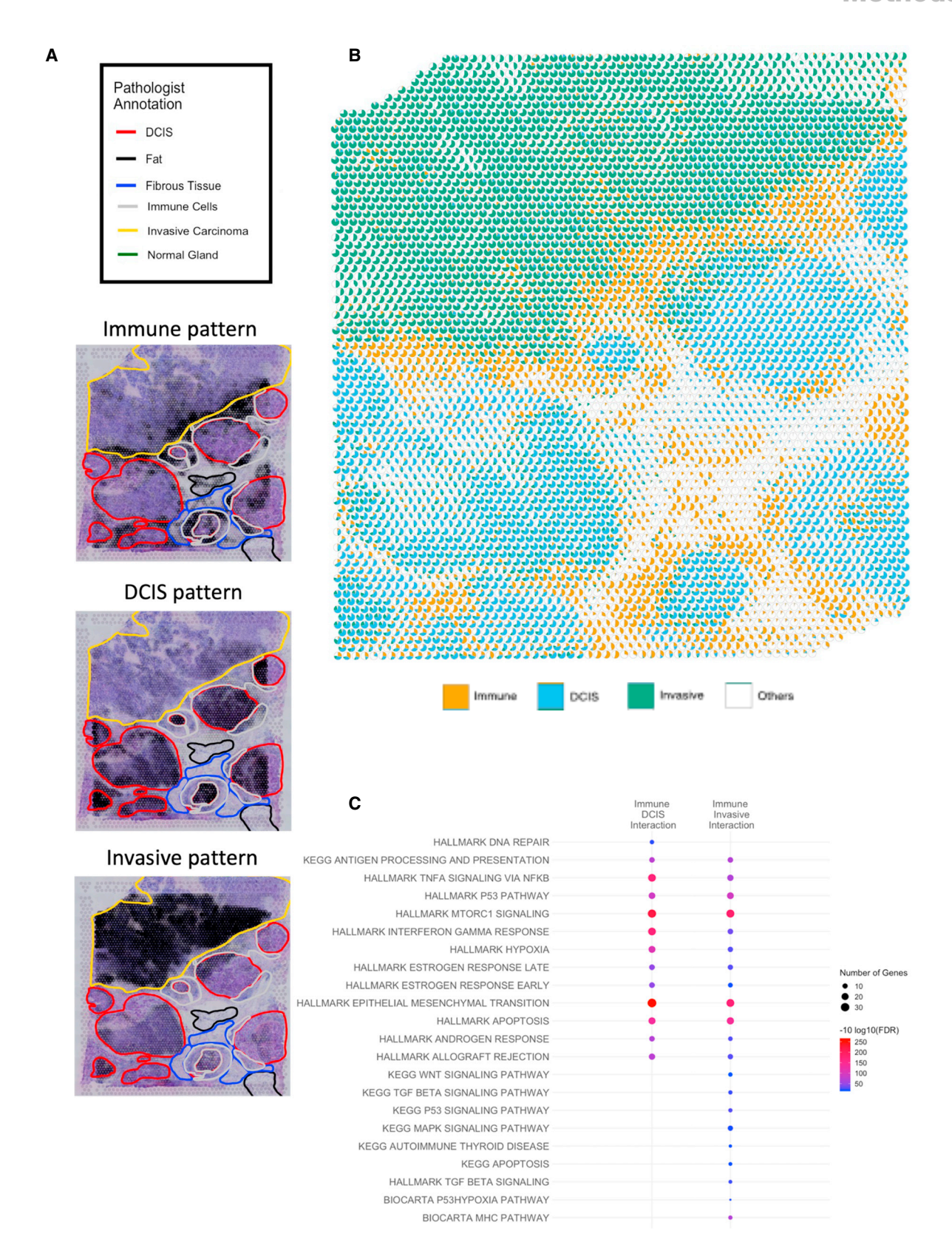
⁽C) Scatterpie chart showing the overlap between pattern 6 and pattern 9 also illustrated how the acinar cells coincide with the interaction region between the two patterns.

⁽D) Two markers of acinar cells identified among the top SpaceMarkers of interaction between patterns 6 and 9 also show overexpression in their interaction region.

⁽E) Overrepresented pathways associated with neoplasia-stromal interactions identified by SpaceMarkers analysis in DE mode demonstrate overrepresentation of acinar cell markers.

⁽F) Other relevant pathways are overrpresented in comparison with acinar markers with the SpaceMarkers analysis in the residual mode. See also Figure S2.





(legend on next page)



genes identified from applying a similar analysis based on the DE for the same FDR value (Data S1). This reduction in the number of markers through the analysis of CoGAPS residuals relative to the inference of SpaceMarkers through the DE analysis is consistent with the isolation of specific nonlinear changes resulting from interactions between the cellular processes measured in the CoGAPS patterns using this mode. We note that 85 of the SpaceMarkers were associated with immune cell interactions in both the invasive carcinoma and DCIS regions. The SpaceMarkers optParams values are tabulated in Table S1. To further determine the molecular pathways activated through immune and tumor cell interactions in both regions, we performed gene set overrepresentation analyses from the Hallmark, KEGG, and Biocarta molecular pathways using the MSigDB, with a selection of the pathways presented in Figure 4C (see Table S4 for the complete list of pathways). We find that although certain pathways were enriched in both interactions (e.g., antigen processing and presentation, p53 pathway, Tnf-alpha signaling, mTorc1 signaling, epithelial to mesenchymal transition, Interferon Gamma response, hypoxia, and estrogen response early/ late), others were enriched exclusively in immune-DCIS (DNA repair) and immune-invasive (WNT signaling, MAPK signaling, and TGF beta signaling), respectively. Note that a pathway enriched in both immune-DCIS and immune-invasive carcinoma interactions may have distinct gene subsets associated with each interaction. For example, it is readily evident that the hallmark interferon-gamma response gene set has greater overlap with the SpaceMarkers of the Immune-DCIS interaction compared with the immune-invasive interaction.

Using SpaceMarkers with high-resolution CoGAPS reveals greater heterogeneity in intercellular interactions within the TME

In all cases presented, the SpaceMarkers inferred fundamentally depend on the resolution of the cellular processes inferred in the CoGAPS latent space analysis. Indeed, nonlinear interactions in interacting regions at a low-resolution analysis may be further refined by increasing the dimensionality of the factorization on the ST data consistent with the recent advances to multi-resolution matrix factorization. 33 We further performed a higher-resolution CoGAPS analysis of the breast cancer data to test whether the interaction region between two patterns and the associated SpaceMarkers genes is identified by increasing the dimensionality of the latent space analysis. In this higher-dimensional analysis, CoGAPS identifies 16 distinct patterns associated with the diverse biological processes in the TME. The activity levels of a selection of the patterns overlaid on an H&E stained slide of the sample are shown in Figure 5A (also see Figure S3). Although the higher number of patterns reveals greater heterogeneity of the biological processes in the sample by further resolving patterns identified in the low-resolution analysis, it does not identify patterns specific to the interactions identified between the lower dimension patterns.

Although we do not associate each Visium spot with solely one pattern, studying the most dominant pattern in spots informs us of the dominant biological process at that location in the tissue as inferred by CoGAPS. Consequently, the same spots are associated with broader biological processes at a lower resolution and with more specific processes at a higher resolution. The alluvial plot in Figure 5B shows the relationship between the most dominant low- and high-resolution patterns at each spot.

For example, the single DCIS-related pattern in Figure 4A resolves into multiple DCIS patterns, some of which are associated with individual DCIS lesions. Even within the single invasive carcinoma lesion, the low-resolution invasive carcinoma pattern resolves into two distinct patterns, one of which is isolated to the interior of the invasive carcinoma and one that spans to the tumor-immune boundary. Although the DCIS lesions and invasive carcinoma have universally high ERBB2 and ESR1 expressions, evaluating the genes associated with the distinct patterns identifies heterogeneity in growth factor signaling pathways with enhanced IGFBP3 expression in the DCIS.5 pattern, FGFR4 expression in the DCIS.6 pattern, and FGFR1 expression in the Invasive.2 carcinoma pattern (Figure S3; Table S5) We also see spots previously associated with the immune pattern or with dispersed patterns at the low resolution now being associated with a dominant pattern that can be associated with the stromal region. To further compare the enhanced resolution intra-tumor heterogeneity to tumor-immune interactions in the high-resolution factorization, Figure 5C shows relative pattern weights and overlap between the immune pattern and the two invasive patterns. It is clear that only one of the invasive patterns overlaps with the immune pattern, thus contributing to the tumor-immune interaction. Still, both of these interacting patterns contain substantial numbers of spots that are isolated to the immune and invasive carcinoma regions, respectively, suggesting that increasing the resolution of the factorization does not compensate for the estimation of nonlinear effects through the interaction statistic. Similarly, Figure 5D shows relative pattern weights and overlap between the immune pattern and the three DCIS patterns. It logically follows that the overlapping regions of the distinct DCIS patterns are also distinct and hence correspond to different molecular alterations from DCIS-immune interactions that will affect the subsequent outgrowth of these distinct lesions.

For these interactions involving the immune pattern, we identify SpaceMarkers genes associated with the inter-pattern interactions as the genes having higher CoGAPS residuals in the interaction region compared with regions with exclusive influence from the individual patterns (Data S1). The SpaceMarkers optParams values are tabulated in Table S1. On the identification of statistically significant (FDR < 0.05) signaling pathways

Figure 4. Low-resolution CoGAPS and SpaceMarkers analysis identifies markers of interaction between broad patterns in breast cancer

⁽A) Images of the breast cancer tissue showing activity levels of the immune, DCIS, and invasive carcinoma patterns, respectively, overlaid on annotated H&E slides showing regions with invasive carcinoma, DCIS lesions, immune cells, and stroma.

⁽B) Scatterpie visualization shows the relative activity levels and overlap between the invasive carcinoma (green), immune (orange), DCIS (blue), and all other patterns combined (white).

⁽C) Overrepresented pathways associated with DCIS-immune interactions and cancer-immune interactions (FDR < 0.05).



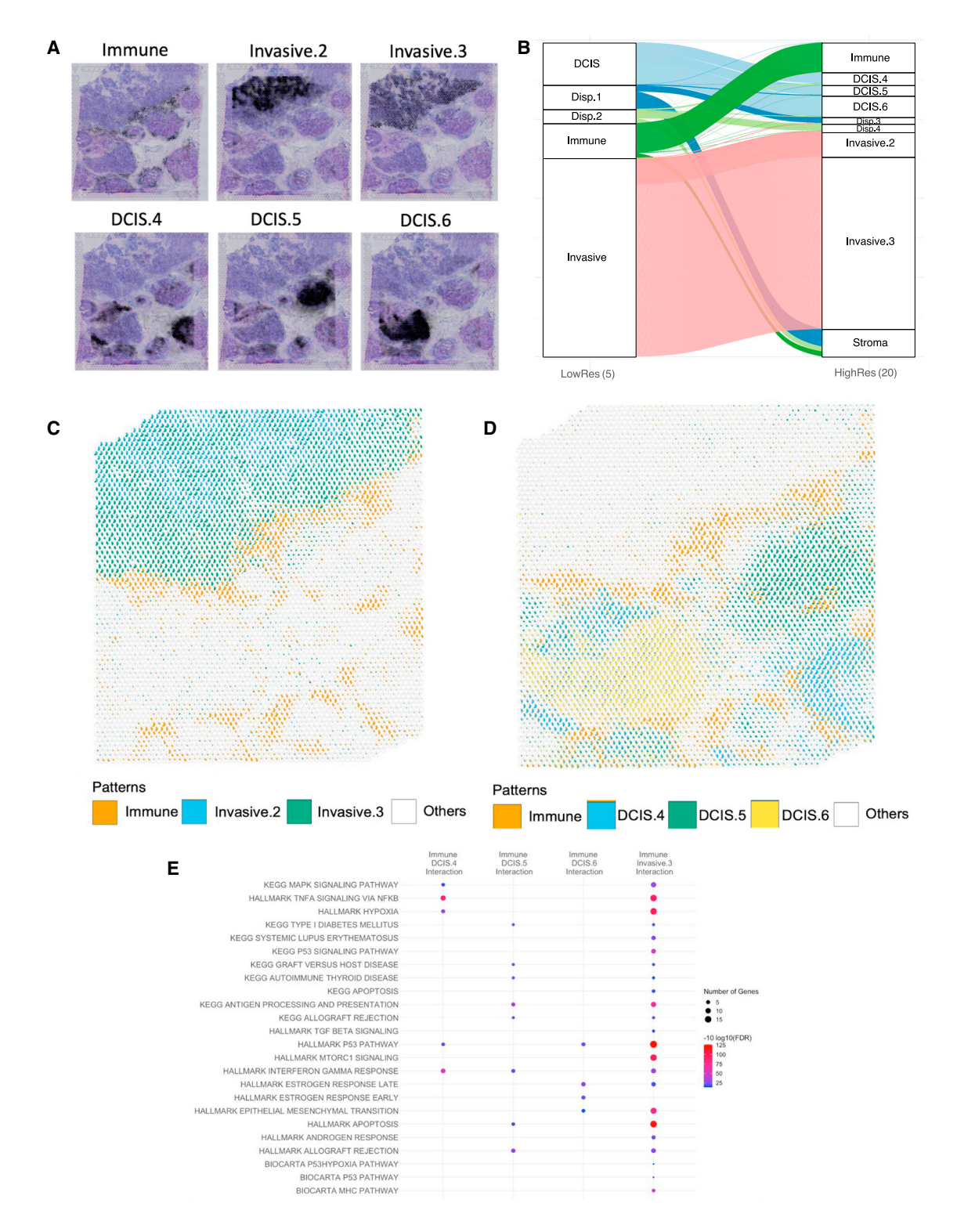


Figure 5. High-resolution CoGAPS and SpaceMarkers analysis of breast cancer tissue reveal greater heterogeneity in intercellular inter-

(A) Multiple patterns associated with invasive carcinoma and DCIS regions identified in higher-resolution CoGAPS analysis with 16 patterns highlights the heterogeneity in the tumor and TME by further resolving the underlying pathology (see Figure S3 for remaining patterns).

(B) Alluvial plot showing the most dominant pattern associated with each spot using low-resolution and high-resolution CoGAPS, respectively. Spots dominated by low-resolution DCIS pattern are dominated by three distinct DCIS-related patterns associated with different lesions in the high-resolution analysis. Invasive



(see Table S4) pertaining to the interaction of the immune pattern with invasive carcinoma and DCIS patterns in the high-dimensional CoGAPS results and comparing them with those found in 5 dimensions, we find pathways common to all interactions and unique to specific pattern interactions. For example, we find 59 signaling pathways enriched due to immune-invasive carcinoma interaction in 5 dimensions and 16 dimensions. These include but are not limited to the pathways related to epithelialmesenchymal transition, apoptosis, antigen processing and presentation, hypoxia, p53 signaling, interferon-alpha and -gamma responses, and finally targets of the oncogene MYC. However, the higher-resolution analysis also reveals unique pathways relevant to specific immune-invasive carcinoma pattern interactions. We found pathways related to the cancer-immune interactions including those related to IL-5 and IL-6 signaling, KRAS signaling, Toll-like receptor signaling, and the CDC25 pathway exclusively when the dominant invasive carcinoma pattern (Invasive.3) interacts with the immune cells. Similarly, the distinct immune-DCIS interactions reveal heterogeneity in the enriched pathways that were not evident with a single DCIS pattern using low-resolution CoGAPS. Among the immune interactions with different DCIS lesions, MAPK signaling, Tnf alpha signaling, and hypoxia pathways, known to be mechanisms of resistance to endocrine and immunotherapies, are enriched exclusively in the immune-DCIS.4 interaction; antigen processing, allograft rejection, and autoimmunity-related pathways are enriched exclusively in immune-DCIS.5; and EMT pathway and estrogen response early/late are exclusively enriched in the immune DCIS.6 interactions. These pathways are consistent with the heterogeneity of subsequent outgrowth of these DCIS lesions, with successful activation of pathways associated with the immune attack in DCIS.5 relative to the invasive processes observed in both DCIS.4 and DCIS.6.

Finally, in addition to the SpaceMarkers analysis of interacting CoGAPS patterns, we also performed cell deconvolution using STdeconvolve¹⁷ to identify cell populations abundant in the invasive carcinoma and DCIS lesions, respectively, and the immune cells (Figure S4). We used SpaceMarkers to identify the markers of interaction between immune cells and the cell populations found to be spatially interacting with them (Data S1). The SpaceMarkers optParams values are tabulated in Table S1.

Integrated ST and single-cell RNA-seq analysis identifies cell type-specific molecular changes from immunotherapy treatment in hepatocellular carcinoma

In the examples so far, the SpaceMarkers statistic revealed the molecular changes associated with intercellular interactions. Since SpaceMarkers relies on spot-based co-localization, it limits the ability to identify the cell subtypes in which these mo-

lecular changes were induced. Transfer learning allows us project new data into learned latent spaces, subsequently associating samples from the new data with known biology. We first factorize the ST data collected from a resected hepatocellular carcinoma (HCC) tumor after the administration of a neoadjuvant cabozantinib and nivolumab therapy to obtain 9 CoGAPS patterns. Figure 6A shows the individual tumor and immune-associated patterns overlaid on an H&E-stained image of the HCC tumor sample. As in the other examples, these tumor and immune patterns are spatially overlapping (Figure 6B) and are deemed to be interacting in regions where they have overlapping influence. This analysis identifies two distinct tumor cell patterns, one of which spans all malignant regions in the sample (pattern 2) and the other isolated to a specific region (pattern 1) that has less co-localization of the immune cells (pattern 8). The interaction between the immune cells and each of the tumor patterns learned through SpaceMarkers identifies enhanced expressions of hepatocyte markers (KRT18, SERPIN family genes, APOC2, CD24), immune markers (CD63, HLA genes), and cell death markers (TNF pathway associated genes, ribosomal genes, ANXA2) consistent with the killing of tumor cells through immune cells in the interaction between patterns 2 and 8 (Data S1). By contrast, SpaceMarkers genes of the interaction between patterns 1 and 8 identify fibroblast markers (collagen coding genes, MYL9, TAGLN) consistent with a lack of successful immune attack and infiltration in this portion of the tumor. The SpaceMarkers optParams values are tabulated in Table S1.

Although the SpaceMarkers analysis of ST data suggests the molecular changes associated with cell-cell interactions, this analysis alone does not pinpoint the precise cells in which these molecular changes occur. By transfer learning^{24,26} of these latent features into matched single-cell RNA-seq data from the same tumor, we can associate individual cells with specific patterns corresponding to tumor and immune signatures (Figure 6C). This association can both identify whether a SpaceMarkers gene's expression changes in tumor or immune cells and whether we can also predict the precise subpopulations of tumor and immune cells involved in intercellular interactions by observing the gene expression changes of the relevant SpaceMarkers in individual cells. From Figure 6D, we observe that changes in the expressions of genes SERPINC1, APOC2, and ADH1B are induced in a subset of the cancer cells attributed to pattern 2, whereas the expression changes in gene PFN1 and CD14 are induced in a subset of the immune cells. A further subset of both pattern 2 tumor cells and immune cells co-express HSP90AA1 and ribosomal genes. Based on these gene expression patterns of the respective SpaceMarkers, we hypothesize that these individual cells are sourced from the tumor-immune boundary. Note that although the analysis in this section

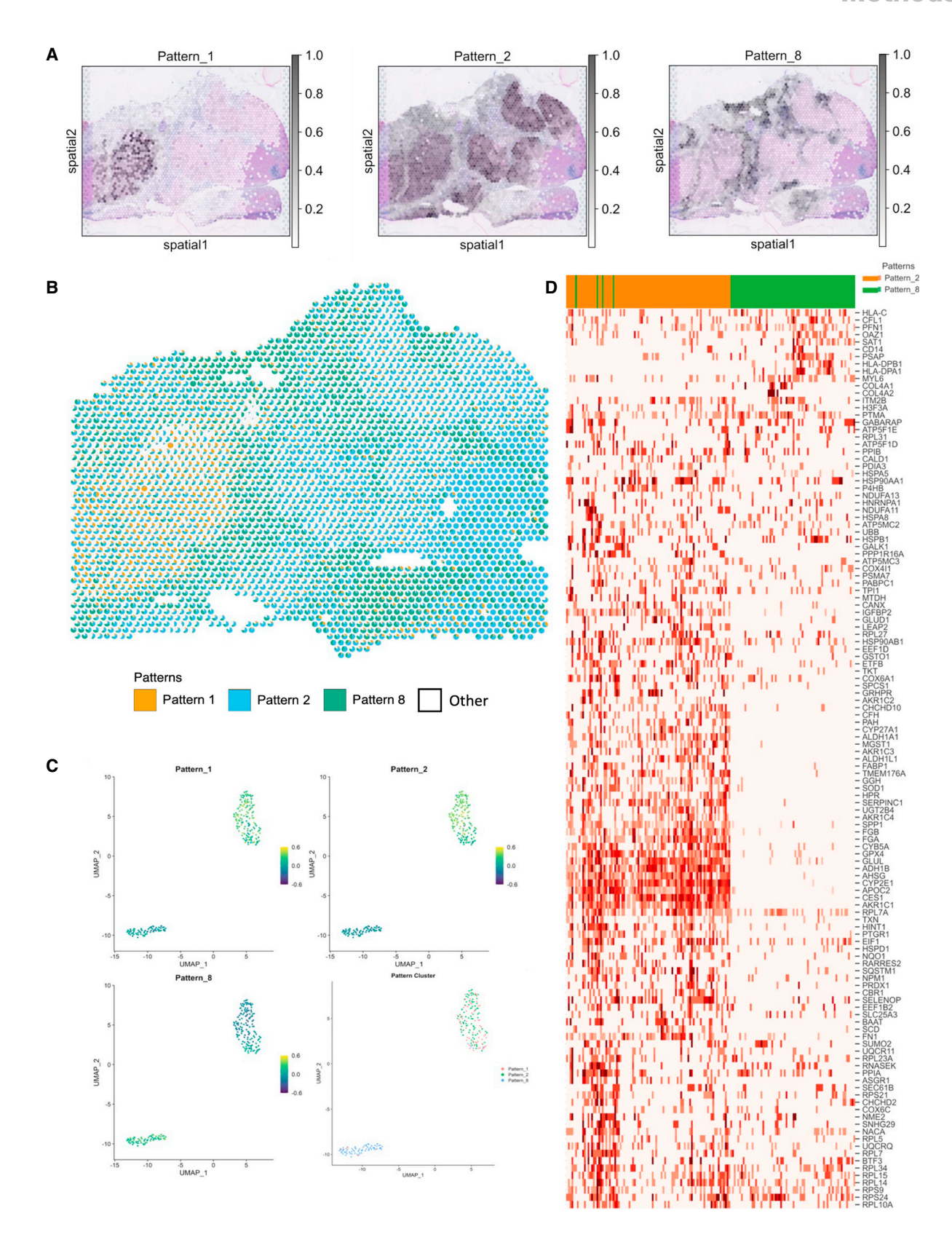
pattern in low resolution resolves into three invasive carcinoma related patterns associated with varying levels of immune infiltration in the high-resolution analysis. For alluvial plot with all 16 patterns, see Figure S4A.

⁽C) Relative activity levels of immune patterns with two invasive patterns reveals that the immune (orange) and Invasive. 2 (blue) patterns have no overlap, hence do not interact. Immune interaction with Invasive Carcinoma (green) is captured through the overlap between Immune and Invasive. 3 pattern. White represents all other patterns combined.

⁽D) Relative activity levels of immune pattern (orange) with three DCIS patterns (blue, green, and yellow) associated with separate lesions reveals distinct overlapping regions associated with each interaction. White represents all other patterns combined.

⁽E) SpaceMarkers of Immune-DCIS and Immune-Invasive interactions reveal functional heterogeneity of the enriched pathways mirroring the spatial heterogeneity revealed in (C) and (D) (FDR < 0.05) (see Table S4 for complete list of gene sets).





(legend on next page)



demonstrated the interaction between the dominant patterns (1, 2, and 8), some of the less-dominant patterns could represent rare cell types or minor biological processes that are essential to the tumor progression and immune response. Accordingly, users should include such patterns for SpaceMarkers analysis in their workflow if needed.

DISCUSSION

We demonstrate how the co-localization of multiple cellular processes in spatial transcriptomics data can be leveraged as an asset to infer molecular changes resulting from cell-cell interactions. Specifically, this inference is enabled through SpaceMarkers, an algorithm for identifying genes associated with pairs of spatially interacting latent features that represent distinct cellular processes. We accomplish this by first identifying a region of influence for each latent feature in the vicinity of spots with high feature activity. Two features are deemed to be interacting in spots where they have a concurrent influence. The SpaceMarkers algorithm can estimate molecular changes from spatially interacting cellular processes in two ways-a default residual mode and a DE mode. We demonstrate that the DE mode is able to identify genes with significantly higher expressions in the region where two latent features overlap. However, the DE mode is subject to confounding factors such as variable cell populations and marker association with multiple cell types. We mitigate these confounding effects in the residual mode, where we identify genes with a significantly higher residual error between the original data and its reconstruction in the region of overlap between two latent features. However, this statistic requires a greater number of spots for robust analysis than the DE method. Although we found that this requirement limited the application of the residual model in the case of the smaller lymph node sample with PDAC metastasis, it was generally applicable to the other tumor-immune interactions in our sample cohort. Although the examples used in this paper use spotbased technologies, we note that SpaceMarkers is readily applicable to alternative imaging-based ST technologies that achieve single-cell resolutions. Consequently, the increased spatial resolution of the ST characterization or multi-omics methods for inferring cellular boundaries^{34,35} will enable a broader application of SpaceMarkers for cell-cell interactions.

We validated the SpaceMarkers output against independent tissue classification algorithm^{30,31} and note that if a cell type is entirely occurring within the interaction region, its marker genes will be inferred as a marker of spatial interaction through SpaceMarkers (Figure 3). Although not a direct molecular change in the input cell states, this co-localization of the cell

type exclusively in the interaction region may be a biological effect induced through the TME state induced by the intercellular interactions. We also note that this effect is mitigated to an extent, but not completely removed in the residual mode if some of the learned patterns are associated with that cell type. Ultimately, we leave it to the user to determine which inferences from SpaceMarkers merit further investigation. Future work can also include follow-up experimental studies using *in vitro* 2D/3D cocultures or *in vivo* depletion studies of cell types found in the interaction region to validate the SpaceMarkers output.

Although SpaceMarkers is not optimized for specific cancer types, we notice that the analysis pipeline performs better when inferring cell-cell interactions for the larger volume of cancer cells in breast and liver tumors (Figures 4, 5, and 6) compared with a smaller density of tumor cells surrounding the duct in the pancreatic samples (Figures 2 and 3). We hypothesize that this difference in performance could be due to a combination of factors including the fact that spot-based Visium technology does not capture the minute details of diffuse tumors and their microenvironment, smaller samples resulting in fewer spots for SpaceMarkers analysis. Future work will focus on the application and optimization of SpaceMarkers to spatial data with single-cell or subcellular-level resolution and extend its performance for cancers with different types of tumor structures.

Due to our focus on tumor-immune cell interactions in our biological analyses, the current version of the SpaceMarkers algorithm admits only two overlapping latent features as input. However, this approach is generally applicable to cell-cell inference from ST data across biological contexts and features associated with any cell subtype or cellular feature defined through the latent space analysis. For example, this approach also enables the analysis of the molecular changes from cell-cell interactions between the immune and stromal cells in the breast cancer tissue (Figure S3; Data S1) and between additional cell types in the PanIN sample (Figure 3). In many cases, multiple latent features are co-localized at the same spot. This could result in the same genes being associated with multiple interaction types, although we did not observe such effects in our case studies. Furthermore, many critical intercellular interactions such as cancerassociated fibroblast (CAF)-driven immunosuppression³⁶ result from possible co-localization of multiple cell phenotypes. To address this, future work should extend the application of SpaceMarkers to identify genes associated with multiple overlapping latent features.

We note that our inference of interactions between cellular processes is performed directly from latent space analyses of the ST data, without the need for additional reference datasets

Figure 6. Contextualizing scRNAseq data using SpaceMarkers and transfer learning from matched ST-scRNAseq data in HCC

(A) CoGAPS factorization reveals spatial patterns associated with tumor annotations of tumor and immune cells (see Figure S5).

(B) Scatterpie visualization shows the relative pattern activity levels associated with the spatially overlapping tumor (orange) and immune (blue) patterns in each Visium spot using a pie chart (white represents activity from all other patterns). SpaceMarkers are genes exhibiting nonlinear effects in the residual space of the CoGAPS patterns in the region with tumor-immune overlap.

(C) Transfer learning of patterns 1, 2, and 8 from ST data to matched scRNAseq data. Scatter plot shows projections of the spatial patterns onto individual cells in the scRNAseq data. Individual cells in the scRNAseq data are associated with the pattern having the highest projection in the cell.

(D) Expression heatmap of SpaceMarkers in tumor and immune cells from matched single-cell data from the same tumor provide the spatial context of the individual cells.

See also Figures S5 and S6.





for single-cell resolution 16 or direct estimates of cellular deconvolution. 18 Although our approach is generally applicable to linear latent space estimation methods, the results of our algorithm fundamentally depend on the latent space method selected for the analysis of the ST data. We demonstrate the application of SpaceMarkers to 10x Visium ST data from different cancers, and we identify markers associated with the interaction between latent features associated with different biological processes. In all cases, we observe that the Bayesian matrix factorization method CoGAPS^{22,24,37} can learn latent features that distinguish regions with tumor and immune cells directly from the ST data without reliance on previous knowledge of marker genes, histology annotations, or spatial coordinates. Because CoGAPS uses high-dimensional features to define cellular phenotypes, it can go beyond the discrete cell types learned from H&E through pathology and enable the deconvolution of spots into a more nuanced mix of biological patterns (Figure 4B). Moreover, pathology annotations from H&E imaging can be limited on flash-frozen OCT samples (Figure 4), as they do not preserve cellular morphology.38 In the case of FFPE samples, automated machine learning-based pathology annotations can be used for cell-type identification.³⁰ Creating higher-resolution CoGAPS analysis by increasing the number of latent features inferred from the ST data is able to further resolve the biological signatures, revealing the tissue heterogeneity. These higherdimensional patterns are independent of the interaction regions between the latent features inferred with SpaceMarkers at a lower dimension. This observation suggests that our approach indeed isolates effects due to intercellular interactions rather than unresolved latent features associated with specific cellular processes.

To demonstrate the compatibility of SpaceMarkers with other latent space methods, we have provided an example of its application in DE mode to the output of STdeconvolve (Figure S4). Future work could extend the SpaceMarkers algorithm to additional latent space methods emerging for ST data and include nonlinear regression with terms involving combinations of patterns to supplement the available SpaceMarkers modes. Still, we note that the current modes for SpaceMarkers can readily be applied to nonlinear latent space methods, provided that the low-dimensional features they infer can be associated with a set of weights for each cell through linearization.

The use of SpaceMarkers on the spot-based 10x Visium technology limits direct inference of the specific cell subtypes in which the interactions induce molecular alterations. We demonstrate that transfer learning^{24,26} of the latent features inferred from the CoGAPS analysis of the ST data into matched singlecell RNA-seq data enables us to define the precise cellular subpopulations with gene expression changes in each SpaceMarkers gene. Other approaches mitigate the need for paired data by coordinated expression changes between annotated pairs of ligands and receptors in both spatial and nonspatial single-cell data. Although these approaches directly model the signaling process, they rely on the correspondence between gene expression and protein function and databases of ligand-receptor pairs.³⁹ Coupling spatial data with newer single-cell technologies that isolate interacting cells⁴⁰ can further enhance this inference.

Ultimately, the results of SpaceMarkers depend on the patterns inferred from the latent space method. The biological robustness of the SpaceMarkers statistic relies on the use of patterns associated with significant activity levels as well as a spatial overlap with other patterns of interest. For example, we analyzed the interaction of immune cells with one invasive carcinoma pattern of the three invasive carcinoma patterns learned using the high-resolution CoGAPS analysis. We did not analyze the other two patterns because one was isolated away from the immune pattern and hence had no interactions, and although the other pattern had a spatial overlap with the immune pattern, it had much lower activity levels. For the residual mode to be effectively used, it is important not only just to resolve the ST data into biologically meaningful latent features but also to provide a good fit between the original ST data and its reconstruction from the latent features. In the absence of a good fit. the residual errors contain not only just the effects attributable to inter-feature interaction and the measurement error but also the estimation errors resulting from an overly constrained factorization. In such cases, we recommend using the SpaceMarkers in the DE mode. Similarly, the utility of SpaceMarkers is diminished if the learned latent features do not correspond to individual cell phenotypes or if markers of essential cell types are not represented by any of the learned latent features. Future work can overcome this limitation through semi-supervised learning methods that use cell-type marker expression as a proxy for the latent feature input in the DE mode for SpaceMarkers.

When genes associated with cell-surface interactions and cytokine secretions are grouped together in a latent feature, the assignment of a single kernel-width parameter to the latent feature in the SpaceMarkers algorithm is inconsistent with the varying distances associated with these two types of intercellular interactions. Identification of intercellular interactions in such scenarios requires a mathematical framework for spatially resolved causal inference that models distinct cell types, varying ranges and gradients of influence for cytokine secretions and surface interactions, and spatially resolved expression of individual genes. One such example is MESSI,41 which uses mixtureof-experts and multi-task learning approaches to predict the gene expression in a particular cell type with the help of signaling genes in neighboring cells. Future work integrating these methods with latent features in place of individual genes will both reduce the computational complexity and enhance the biological interpretability of these spatially aware network inference methods.

STAR*METHODS

Detailed methods are provided in the online version of this paper and include the following:

- KEY RESOURCES TABLE
- RESOURCE AVAILABILITY
 - Lead contact
 - Materials availability
 - High-resolution figures
 - Data and code availability
- METHOD DETAILS
 - Sample collection, preparation, and storage

Methods



- ST library preparation
- SpaceMarkers algorithm
- Multi-resolution CoGAPS analysis
- Scatterpie visualizations
- O ProjectR analysis with matched single-cell RNA-
- O Gene Set Enrichment Analysis using MsigDB

SUPPLEMENTAL INFORMATION

Supplemental information can be found online at https://doi.org/10.1016/j. cels.2023.03.004.

ACKNOWLEDGMENTS

We thank Jennifer Durham for facilitating the sample acquisition and data archival process and Ana Cordova for providing valuable inputs for improving the visualizations. This work was supported by NCI F31CA268724-01 (to D.N.S), NIH R01CA138264 (to A.V.F.), R50CA243627 (to L.D.W.), R01CA138264 (to A.S.P.), P01-CA247886 (to E.M.J.), P30CA006973 (to E.M.J.), U01CA212007 (to E.J.F. and A.S.P.), U01CA253403 (to E.J.F.), U54CA274371 (to E.J.F. and L.D.W), U01CA271273 (to E.J.F. and L.D.W.), U01AG060903 (to D.W.), U54CA268083 (to D.W., L.D.W., and A.K.), U54AR081774 (to D.W.), U54CA143868 (to D.W.), and P50CA062924-24A1 (to E.M.J, E.J.F., L.T.K, L.Z., and L.D.W.); NIH K99 NS122085 from BRAIN Initiative in partnership with the National Institute of Neurological Disorders (to G.S.-O.); SU2C/AACR DT-14-14 (to E.M.J.); Lustgarten Foundation Translational Convergence Program Grant (to E.M.J.); Lustgarten Foundation grant (to L.D.W.); the Sol Goldman Pancreatic Cancer Research Center grant (to L.T.K. and L.D.W.); the Emerson Cancer Research Fund (to E.M.J., E.J.F., and W.J.H); an Allegheny Health Network (AHN) grant (to E.J.F. and W.J.H.); Kavli NDS Distinguished Postdoctoral Fellowship (to G.S.-O.); Johns Hopkins Provost Postdoctoral Fellowship (to G.S.-O.); and the JHU Discovery Award (to E.J.F. and L.D.W.).

AUTHOR CONTRIBUTIONS

Conceptualization, A.D. and E.J.F.; methodology, A.D., M.L., E.J.F, G.S.-O., and A.V.F.; software, A.D., M.L., A.T.F.B., S.Z., L.D., and E.J.F.; validation, A.D., M.L., L.D., A.T.F.B., Q.Z., and R.A.A.; formal analysis, A.D., M.L., D.N.S., S.Z., A.T.F.B., L.Y., and A.K.; investigation, A.D., M.L., D.N.S., S.Z., A.T.F.B., L.Y., L.T.K., P.-H.W., K.F., Q.Z., and E.J.F; resources, S.R.W., C.R.U., J.C., A.H., Z.W.B., E.M.J., L.Z., L.T.K., M.Y., and L.D.W.; data curation,S.R.W., C.R.U., J.C., A.H., Z.W.B., L.D.W., and L.T.K.; writing - original draft, A.D., M.L., D.N.S., S.Z., L.Y., A.T.F.B., Q.Z., W.J.H., C.S.-M., D.M.G., S.R.W., C.R.U., J.C., A.H., Z.W.B., A.V.F., A.S.P., M.Y., A.K., P.-H.W., K.F., D.W., L.D.W., L.Z., E.M.J., R.A.A., L.D., G.S.-O., L.T.K., and E.J.F.; writing - review & editing, A.D., M.L., D.N.S., S.Z., L.Y., A.T.F.B., Q.Z., W.J.H., C.S., D.M.G., S.R.W., C.R.U., J.C., A.H., Z.W.B., A.V.F., A.S.P., M.Y., A.K., P.-H.W., K.F., D.W., L.D.W., L.Z., E.M.J., R.A.A., L.D., G.S.-O., L.T.K., and E.J.F.; visualization, A.D., M.L., D.N.S., S.Z., A.T.F.B., L.Y., A.K., E.J.F., and G.S.-O.; supervision, E.J.F. and L.T.K.; project administration, E.J.F.; funding acquisition, E.J.F., E.M.J., L.D.W., and D.W.

DECLARATION OF INTERESTS

E.J.F. is on the Scientific Advisory Board of Viosera Therapeutics and is a paid consultant for Merck and Mestag Therapeutics. W.J.H. reports royalties from Rodeo/Amgen; grants from Sanofi and NeoTX; and consulting fees from Exelixis outside the submitted work. E.M.J. reports other support from Abmeta, personal fees from Achilles, personal fees from DragonFly, other support from Parker Institute, grants and other support from Lustgarten, personal fees from Carta and Bluedot, grants and other support from Genentech, and grants and other support from Break Through Cancer outside the submitted work. S.R.W., C.R.U., J.C., A.H., and Z.W.B. are equity stockholders and employees of 10x Genomics. L.Z. receives grant support from Bristol-Meyer Squibb, Merck, AstraZeneca, iTeos, Amgen, NovaRock, Inxmed, and Halozyme. L.Z. is a paid consultant/Advisory Board Member at Biosion, Alphamab, NovaRock, Ambrx, Akrevia/Xilio, QED, Natera, Novagenesis, Snow Lake Captials, Tempus, Amberston, and Mingruizhiyao. L.Z. holds shares at Alphamab and Mingruizhiyao. M.Y. reports grants and research support from Bristol-Myers Squibb, Incyte, and Genentech as well as honoraria from Genentech, Exelixis, Eisai, AstraZeneca, Replimune, and Hepion. C.S.M. reports research funding from Pfizer, AstraZeneca, BMS, and GSK/Tesaro and serves on the advisory boards of Bristol Myers Squibb (not paid), Seattle Genetics, Genomic Health, and Athenex. R.A.A. receives research support from Bristol-Myers Squibb, RAPT therapeutics, Stand up to Cancer, and the National Institutes of Health and serves on the advisory boards for Bristol-Myers Squibb, Merck SD, and AstraZeneca. A.S.P. is a consultant to AsclepiX Therapeutics and CytomX Therapeutics; he is the founder and Chief Scientific Advisor of AsclepiX Therapeutics; he receives research grants from AstraZeneca and Boehringer Ingelheim. The terms of these arrangements are being managed by the Johns Hopkins University in accordance with its conflict-of-interest policies.

INCLUSION AND DIVERSITY

We support inclusive, diverse, and equitable conduct of research.

Received: May 17, 2022 Revised: July 26, 2022 Accepted: March 20, 2023

Published: April 19, 2023; corrected: July 25, 2023

REFERENCES

- 1. Seo, H.R. (2015). Roles of tumor microenvironment in hepatocelluar carcinoma. Curr. Med. Chem. 11, 82-93. https://doi.org/10.2174/1573394711 666151022203313.
- 2. Davis-Marcisak, E.F., Deshpande, A., Stein-O'Brien, G.L., Ho, W.J., Laheru, D., Jaffee, E.M., Fertig, E.J., and Kagohara, L.T. (2021a). From bench to bedside: single-cell analysis for cancer immunotherapy. Cancer Cell 39, 1062-1080. https://doi.org/10.1016/j.ccell.2021.07.004.
- 3. Juengpanich, S., Topatana, W., Lu, C., Staiculescu, D., Li, S., Cao, J., Lin, J., Hu, J., Chen, M., Chen, J., and Cai, X. (2020). Role of cellular, molecular and tumor microenvironment in hepatocellular carcinoma: possible targets and future directions in the regorafenib era. Int. J. Cancer 147, 1778-1792. https://doi.org/10.1002/ijc.32970.
- 4. Whiteside, T.L. (2008). The tumor microenvironment and its role in promoting tumor growth. Oncogene 27, 5904-5912. https://doi.org/10.1038/onc. 2008.271.
- 5. Dhanasekaran, R., Baylot, V., Kim, M., Kuruvilla, S., Bellovin, D.I., Adeniji, N., Rajan Kd, A., Lai, I., Gabay, M., Tong, L., et al. (2020). MYC and twist1 cooperate to drive metastasis by eliciting crosstalk between cancer and innate immunity. eLife 9, e50731. https://doi.org/10.7554/eLife.50731.
- 6. Fu, L.Q., Du, W.L., Cai, M.H., Yao, J.Y., Zhao, Y.Y., and Mou, X.Z. (2020). The roles of tumor-associated macrophages in tumor angiogenesis and metastasis. Cell. Immunol. 353, 104119. https://doi.org/10.1016/j.cellimm.2020.104119.
- 7. Wei, C., Yang, C., Wang, S., Shi, D., Zhang, C., Lin, X., Liu, Q., Dou, R., and Xiong, B. (2019). Crosstalk between cancer cells and tumor associated macrophages is required for mesenchymal circulating tumor cell-mediated colorectal cancer metastasis. Mol. Cancer 18, 64. https://doi.org/ 10.1186/s12943-019-0976-4.
- 8. Chaudhary, B., and Elkord, E. (2016). Regulatory T cells in the tumor microenvironment and cancer progression: role and therapeutic targeting. Vaccines 4, 28. https://doi.org/10.3390/vaccines4030028.
- 9. Li, T., Liu, T., Zhu, W., Xie, S., Zhao, Z., Feng, B., Guo, H., and Yang, R. (2021). Targeting MDSC for immune-checkpoint blockade in cancer immunotherapy: current progress and new prospects. Clin. Med. Insights Oncol. 15. 11795549211035540. https://doi.org/10.1177/ 11795549211035540.





- Place, A.E., Jin Huh, S., and Polyak, K. (2011). The microenvironment in breast cancer progression: biology and implications for treatment. Breast Cancer Res. 13, 227. https://doi.org/10.1186/bcr2912.
- Soysal, S.D., Tzankov, A., and Muenst, S.E. (2015). Role of the tumor microenvironment in breast cancer. Pathobiology 82, 142–152. https:// doi.org/10.1159/000430499.
- Rao, N., Clark, S., and Habern, O. (2020). Bridging genomics and tissue pathology. Genet. Eng. Biotechnol. News 40, 50–51. https://doi.org/10. 1089/gen.40.02.16.
- Wu, S.Z., Al-Eryani, G., Roden, D.L., Junankar, S., Harvey, K., Andersson, A., Thennavan, A., Wang, C., Torpy, J.R., Bartonicek, N., et al. (2021). A single-cell and spatially resolved atlas of human breast cancers. Nat. Genet. 53, 1334–1347. https://doi.org/10.1038/s41588-021-00911-1.
- Ji, A.L., Rubin, A.J., Thrane, K., Jiang, S., Reynolds, D.L., Meyers, R.M., Guo, M.G., George, B.M., Mollbrink, A., Bergenstråhle, J., et al. (2020). Multimodal analysis of composition and spatial architecture in human squamous cell carcinoma. Cell 182, 497–514.e22. https://doi.org/10. 1016/j.cell.2020.05.039.
- Andersson, A., Larsson, L., Stenbeck, L., Salmén, F., Ehinger, A., Wu, S.Z., Al-Eryani, G., Roden, D., Swarbrick, A., Borg, Å., et al. (2021). Spatial deconvolution of HER2-positive breast cancer delineates tumor-associated cell type interactions. Nat. Commun. 12, 6012. https://doi.org/10.1038/ s41467-021-26271-2.
- Cable, D.M., Murray, E., Zou, L.S., Goeva, A., Macosko, E.Z., Chen, F., and Irizarry, R.A. (2022). Robust decomposition of cell type mixtures in spatial transcriptomics. Nat. Biotechnol. 40, 517–526. https://doi.org/10. 1038/s41587-021-00830-w.
- Miller, B.F., Huang, F., Atta, L., Sahoo, A., and Fan, J. (2021). Referencefree cell-type deconvolution of multi-cellular pixel-resolution spatially resolved transcriptomics data. Nat. Commun. 13, 2339. https://doi.org/ 10.1101/2021.06.15.448381.
- Zhao, E., Stone, M.R., Ren, X., Guenthoer, J., Smythe, K.S., Pulliam, T., Williams, S.R., Uytingco, C.R., Taylor, S.E.B., Nghiem, P., et al. (2021). Spatial transcriptomics at subspot resolution with BayesSpace. Nat. Biotechnol. 39, 1375–1384. https://doi.org/10.1038/s41587-021-00935-2.
- Hu, J., Li, X., Coleman, K., Schroeder, A., Ma, N., Irwin, D.J., Lee, E.B., Shinohara, R.T., and Li, M. (2021). SpaGCN: integrating gene expression, spatial location and histology to identify spatial domains and spatially variable genes by graph convolutional network. Nat. Methods 18, 1342–1351. https://doi.org/10.1038/s41592-021-01255-8.
- Elosua-Bayes, M., Nieto, P., Mereu, E., Gut, I., and Heyn, H. (2021). SPOTlight: seeded NMF regression to deconvolute spatial transcriptomics spots with single-cell transcriptomes. Nucleic Acids Res. 49, e50. https://doi.org/10.1093/nar/gkab043.
- Luca, B.A., Steen, C.B., Matusiak, M., Azizi, A., Varma, S., Zhu, C., Przybyl, J., Espín-Pérez, A., Diehn, M., Alizadeh, A.A., et al. (2021). Atlas of clinically distinct cell states and ecosystems across human solid tumors. Cell 184, 5482–5496.e28. https://doi.org/10.1016/j.cell.2021. 09.014.
- Fertig, E.J., Ding, J., Favorov, A.V., Parmigiani, G., and Ochs, M.F. (2010).
 CoGAPS: an R/C++ package to identify patterns and biological process activity in transcriptomic data. Bioinformatics 26, 2792–2793. https://doi.org/10.1093/bioinformatics/btq503.
- Davis-Marcisak, E.F., Fitzgerald, A.A., Kessler, M.D., Danilova, L., Jaffee, E.M., Zaidi, N., Weiner, L.M., and Fertig, E.J. (2021b). Transfer learning between preclinical models and human tumors identifies a conserved NK cell activation signature in anti-CTLA-4 responsive tumors. Genome Med. 13, 129. https://doi.org/10.1186/s13073-021-00944-5.
- Stein-O'Brien, G.L., Clark, B.S., Sherman, T., Zibetti, C., Hu, Q., Sealfon, R., Liu, S., Qian, J., Colantuoni, C., Blackshaw, S., et al. (2019). Decomposing cell identity for transfer learning across cellular measure-ments, platforms, tissues, and species. Cell Syst. 8, 395–411.e8. https://doi.org/10.1016/j.cels.2019.04.004.
- Stein-O'Brien, G.L., Arora, R., Culhane, A.C., Favorov, A.V., Garmire, L.X., Greene, C.S., Goff, L.A., Li, Y., Ngom, A., Ochs, M.F., et al. (2018). Enter

- the matrix: factorization uncovers knowledge from omics. Trends Genet. 34, 790–805. https://doi.org/10.1016/j.tig.2018.07.003.
- Sharma, G., Colantuoni, C., Goff, L.A., Fertig, E.J., and Stein-O'Brien, G. (2020). projectR: an R/Bioconductor package for transfer learning via PCA, NMF, correlation and clustering. Bioinformatics 36, 3592–3593. https://doi.org/10.1093/bioinformatics/btaa183.
- Liberzon, A., Subramanian, A., Pinchback, R., Thorvaldsdóttir, H., Tamayo, P., and Mesirov, J.P. (2011). Molecular signatures database (MSigDB) 3.0. Bioinformatics 27, 1739–1740. https://doi.org/10.1093/bio-informatics/btr260.
- Subramanian, A., Tamayo, P., Mootha, V.K., Mukherjee, S., Ebert, B.L., Gillette, M.A., Paulovich, A., Pomeroy, S.L., Golub, T.R., Lander, E.S., and Mesirov, J.P. (2005). Gene set enrichment analysis: a knowledgebased approach for interpreting genome-wide expression profiles. Proc. Natl. Acad. Sci. USA 102, 15545–15550. https://doi.org/10.1073/pnas. 0506580102.
- Liberzon, A., Birger, C., Thorvaldsdóttir, H., Ghandi, M., Mesirov, J.P., and Tamayo, P. (2015). The Molecular Signatures Database (MSigDB) hallmark gene set collection. Cell Syst. 1, 417–425. https://doi.org/10.1016/j.cels. 2015.12.004.
- Bell, A.T., Mitchell, J.T., Kiemen, A.L., Fujikura, K., Fedor, H., Gambichler, B., Deshpande, A., Wu, P.-H., Sidiropoulos, D.N., Erbe, R., et al. (2022). PanIN and CAF transitions in pancreatic carcinogenesis revealed with spatial data integration. Preprint at bioRxiv. https://doi.org/10.1101/ 2022.07.16.500312.
- Kiemen, A.L., Braxton, A.M., Grahn, M.P., Han, K.S., Babu, J.M., Reichel, R., Jiang, A.C., Kim, B., Hsu, J., Amoa, F., et al. (2022). CODA: quantitative 3D reconstruction of large tissues at cellular resolution. Nat. Methods 19, 1490–1499. https://doi.org/10.1038/s41592-022-01650-9.
- Segerstolpe, Å., Palasantza, A., Eliasson, P., Andersson, E.M., Andréasson, A.C., Sun, X., Picelli, S., Sabirsh, A., Clausen, M., Bjursell, M.K., et al. (2016). Single-cell transcriptome profiling of human pancreatic islets in health and Type 2 diabetes. Cell Metab. 24, 593–607. https://doi. org/10.1016/j.cmet.2016.08.020.
- Mohammadi, S., Davila-Velderrain, J., and Kellis, M. (2020). A multiresolution framework to characterize single-cell state landscapes. Nat. Commun. 11, 5399. https://doi.org/10.1038/s41467-020-18416-6.
- Biancalani, T., Scalia, G., Buffoni, L., Avasthi, R., Lu, Z., Sanger, A., Tokcan, N., Vanderburg, C.R., Segerstolpe, Å., Zhang, M., et al. (2021).
 Deep learning and alignment of spatially resolved single-cell transcriptomes with Tangram. Nat. Methods 18, 1352–1362. https://doi.org/10.1038/s41592-021-01264-7.
- Pham, D.T., Tan, X., Xu, J., Grice, L.F., Lam, P.Y., Raghubar, A., et al. (2020). stLearn: integrating spatial location, tissue morphology and gene expression to find cell types, cell-cell interactions and spatial trajectories within undissociated tissues. Preprint at bioRxiv. https://doi.org/10.1101/2020.05.31.125658v1.
- Monteran, L., and Erez, N. (2019). The dark side of fibroblasts: cancerassociated fibroblasts as mediators of immunosuppression in the tumor microenvironment. Front. Immunol. 10, 1835. https://doi.org/10.3389/ firmus.2019.01835
- Sherman, T.D., Gao, T., and Fertig, E.J. (2020). CoGAPS 3: Bayesian nonnegative matrix factorization for single-cell analysis with asynchronous updates and sparse data structures. BMC Bioinformatics 21, 453. https:// doi.org/10.1186/s12859-020-03796-9.
- Cox, M.L., Schray, C.L., Luster, C.N., Stewart, Z.S., Korytko, P.J., M Khan, K.N., Paulauskis, J.D., and Dunstan, R.W. (2006). Assessment of fixatives, fixation, and tissue processing on morphology and RNA integrity. Exp. Mol. Pathol. 80, 183–191. https://doi.org/10.1016/j.yexmp.2005.10.002.
- Efremova, M., Vento-Tormo, M., Teichmann, S.A., and Vento-Tormo, R. (2020). CellPhoneDB: inferring cell-cell communication from combined expression of multi-subunit ligand-receptor complexes. Nat. Protoc. 15, 1484–1506. https://doi.org/10.1038/s41596-020-0292-x.
- 40. Giladi, A., Cohen, M., Medaglia, C., Baran, Y., Li, B., Zada, M., Bost, P., Blecher-Gonen, R., Salame, T.M., Mayer, J.U., et al. (2020). Dissecting



- cellular crosstalk by sequencing physically interacting cells. Nat. Biotechnol. 38, 629-637. https://doi.org/10.1038/s41587-020-0442-2.
- 41. Li, D., Ding, J., and Bar-Joseph, Z. (2021). Identifying signaling genes in spatial single cell expression data. Bioinformatics 37, 968-975. https:// doi.org/10.1093/bioinformatics/btaa769.
- 42. Hao, Y., Hao, S., Andersen-Nissen, E., Mauck, W.M., Zheng, S., Butler, A., Lee, M.J., Wilk, A.J., Darby, C., Zager, M., et al. (2021). Integrated analysis of multimodal single-cell data. Cell 184, 3573-3587.e29. https://doi.org/ 10.1016/j.cell.2021.04.048.
- 43. Ho, W.J., Zhu, Q., Durham, J., Popovic, A., Xavier, S., Leatherman, J., Mohan, A., Mo, G., Zhang, S., Gross, N., et al. (2021). Neoadjuvant cabozantinib and nivolumab convert locally advanced hepatocellular carcinoma into resectable disease with enhanced antitumor immunity. Nat. Cancer 2, 891-903. https://doi.org/10.1038/s43018-021-00234-4.
- 44. Baddeley, A., Rubak, E., and Turner, R. (2015). Spatial Point Patterns: Methodology and Applications with R (Chapman and Hall/ CRC Press).
- 45. Kruskal, W.H., and Wallis, W.A. (1952). Use of ranks in One-Criterion variance analysis. J. Am. Stat. Assoc. 47, 583-621. https://doi.org/10.1080/ 01621459.1952.10483441.
- 46. Dunn, O.J. (1964). Multiple comparisons using rank sums. Technometrics 6, 241-252. https://doi.org/10.1080/00401706.1964.10490181.
- 47. Hafemeister, C., and Satija, R. (2019). Normalization and variance stabilization of single-cell RNA-seq data using regularized negative binomial regression. Genome Biol. 20, 296. https://doi.org/10.1186/s13059-019-1874-1.





STAR*METHODS

KEY RESOURCES TABLE

REAGENT or RESOURCE	SOURCE	IDENTIFIER	
Deposited data			
Processed spatial and single-cell transcriptomics data.	This paper.	GEO:GSE224411	
Software and algorithms			
SpaceMarkers v0.81	This paper.	https://doi.org/10.5281/zenodo.7621285	
SpaceMarkers analysis scripts.	This paper.	https://doi.org/10.5281/zenodo.7621291	
STdeconvolve	Miller et al., 2022 ¹⁷	https://github.com/JEFworks-Lab/ STdeconvolve	
CoGAPS v3.15.2	Sherman et al. ³⁷	https://doi.org/10.18129/B9.bioc.CoGAPS	
projectR v1.6.0	Sharma et al., 2022 ²⁶	https://doi.org/10.18129/B9.bioc.projectR	
GSEA	Subramanian et al. ²⁸ ; https://www.gsea-msigdb.org/	GSEA v4.2.3	
Seurat v4.1.0	Hao et al., 2021 ⁴²	Version 4.1.0	
Other			
Gene sets	www.msigdb.com	MSigDB v7.5.1 (Hallmark, Biocarta, and Kegg)	
High resolution figures	This paper.	https://doi.org/10.5281/zenodo.7622690	

RESOURCE AVAILABILITY

Lead contact

Further information and requests for resources and reagents should be directed to and will be fulfilled by the lead contact, Elana J Fertig (ejfertig@jhmi.edu)

Materials availability

This study did not generate new materials.

High-resolution figures

High resolution versions of the figures in this manuscript are available on Zenodo (https://doi.org/10.5281/zenodo.7622690).

Data and code availability

- Processed 10x Visium data from the PDAC lymph node, PanIN, and HCC samples have been deposited at the Gene Expression Omnibus (GEO) and are publicly available as of the date of publication. Accession numbers are listed in the key resources table.
- The original code for the SpaceMarkers package is available at www.github.com/FertigLab/SpaceMarkers under MIT license and archived on Zenodo (https://doi.org/10.5281/zenodo.7621285). The scripts used for the analysis presented in this paper is available at www.github.com/atuldeshpande/SpaceMarkers-paper and archived on Zenodo (https://doi.org/10.5281/zenodo.
- Any additional information required to reanalyze the data reported in this paper is available from the lead contact upon request.

METHOD DETAILS

Sample collection, preparation, and storage Invasive breast ductal carcinoma

The fresh frozen invasive breast ductal carcinoma was collected in 2011 and obtained from BioIVT. The tumor was stage IIA, ER Positive, PR Negative, Hercep Test 2+. The RNA quality of the sample, as measured with Bioanalyzer (Agilent) was RIN = 9.26. The sample was embedded in optimal cutting temperature (OCT) compound and immediately frozen. Cryosections of 10 μ m were placed on Visium Gene Expression slides (10x Genomics).



PDAC metastatic lymph node

The PDAC peritumoral lypmh node was surgically resected during curative surgery at the Johns Hopkins University. The lymph node was embedded in OCT and immediately frozen. Pathological examination of an H&E stained cryosection identified a PDAC metastasis to the lymph node. A cryosection of 10 μ m were placed on a Visium Gene Expression slide (10x Genomics).

PanIN sample

The PanIN sample was a surgical specimen from a collection obtained during 2016 to 2018 available in the Johns Hopkins University School of Medicine Department of Pathology archives under Institutional Review Board approval (IRB00274690) under a waiver of consent.

HCC sample

The HCC sample was surgically obtained as part of a clinical trial (NTC03299946) for neoadjuvant cabozantinib and nivolumab previously described. ⁴³ The surgical specimen was immediately embedded in OCT, frozen and a 10 μ m cryosection was placed in a Visium Gene Expression slide (10x Genomics).

ST library preparation

Briefly, following tissue permeabilization optimization, according to 10x Genomics instructions, samples were fixed in methanol, stained (H&E) and imaged. Sequencing libraries were prepared using the Visium Spatial Gene Expression Reagent Kit (10x Genomics), following manufacturer's instructions, and sequenced on an Illumina NovaSeq.

SpaceMarkers algorithm

Here we describe the SpaceMarkers algorithm to identify genes associated with nonlinear effects of latent feature interactions. To facilitate exposition, we will refer to the spatial component of the latent features as "patterns".

Modeling pattern interactions in the residual space

We assume a generic latent space representation model where the ST data matrix *D* is factorized into two low-rank matrices *A* and *P*. Consequently, the matrix product *AP* is a low-rank approximation of the high-dimensional spatial RNAseq data, accounting for all linear combinations of the latent patterns such that

$$D_{ij} \doteq (AP)_{ii} + \varepsilon_{ij}$$
,

where measurement noise ε_{ij} are independent and normally distributed with zero mean (see Fertig et al. ²² for the CoGAPS-specific model). However, this assumption associates the CoGAPS residuals purely with measurement noise, disregarding any molecular changes resulting from inter-pattern interactions. To that end, we introduce an additional term $f(A, P)_{ij}$ which represents the unknown molecular changes due to pattern interactions such that

$$D_{ij} \doteq (AP)_{ij} + f(A, P)_{ij} + \varepsilon_{ij},$$

where the measurement noise ε_{ij} are independent and normally distributed with zero mean and variance σ_{ij}^2 . Thus, we hypothesize that the residuals represent both measurement noise and the molecular changes from inter-pattern interactions. Within the scope of this paper, we seek to only identify genes which exhibit higher residual effects associated with two interacting patterns. To this end, we use CoGAPS with the default settings and analyze the residual space of the CoGAPS factorization results. That is, we use the CoGAPS residuals as an estimate of $f(A, P)_{ij}$ such that

$$\widehat{f}(A,P)_{ij} \doteq E\left[f(A,P)_{ij}\middle|D,A,P\right] = D_{ij} - (AP)_{ij}$$

in regions where two patterns interact (i.e., have overlapping influence) versus regions where each pattern has exclusive influence. To identify the genes associated with the nonlinear interactions between a given pair of patterns, we first identify hotspots of pattern influence for each pattern. If both patterns have overlapping influence in a spot, they are deemed to be interacting in that spot. The CoGAPS residuals are computed in the interacting regions as well as in regions where each pattern is individually active. When the null hypothesis of non-interaction between the patterns is true, the residuals have no dependence on underlying regions (interacting or exclusive). On the other hand, genes associated with higher CoGAPS residuals in the interacting regions compared with the regions with exclusive pattern influence from either pattern show a strong dependence on spatial overlap between the patterns, and thus reject the null hypothesis. These genes constitute the SpaceMarkers, markers of spatial interaction between the two patterns in question. Focusing on strictly higher residuals avoids the confounding factors from decreased gene expression due to heterogeneous spot populations compared to homogeneous ones.

Identifying regions of pattern influence and pattern interaction

For each spatially resolved pattern, we identify its region of influence by using a Gaussian kernel-based spatial smoothing approach. Through the spatial smoothing, we model a pattern's influence extending beyond a spot to its neighboring spots as well. Given the pattern intensity $p(s_i)$ associated with a i-th spot $s_i = (x_i, y_i)$ in the sample, we calculate the spatially smoothed pattern intensities by using the leave-one-out method

$$\widehat{\rho}_{w_p}(s_i) = \sum_{s_j \neq s_i} w_p(s_i, s_j) p(s_j)$$





with the spatial Gaussian kernel

$$w_p(s_i, s_j) = \frac{1}{\sqrt{2\pi}\sigma_{w_p}} e^{\frac{-d(s_i, s_j)^2}{2\sigma_{w_p}^2}},$$

where $d(s_i, s_j) = \sqrt{(x_i - x_j)^2 + (y_i - y_j)^2}$ is the distance between the *i*-th and *j*-th spots, and σ_{w_p} is the kernel width. We used the Smooth.ppp function in the R package spatstat⁴⁴ to perform the smoothing. We obtain a null-distribution by applying the kernelbased smoothing to spatially permuted pattern values (by pseudorandomly assigning spot locations (nperm = 100)). This null-distribution is assumed to be normal, and we obtain the sample mean $\widehat{\mu_p}$ and standard deviation $\widehat{\sigma_p}$ for each pattern. We identify the pattern's region of influence as the set of spots with outliers

$$\widehat{p}_{w_p}(s_i) > \widehat{\mu_p} + \tau_p \widehat{\sigma_p},$$

where τ_D is the outlier threshold for the pattern. The optimal values of the kernel width w_D and outlier threshold τ_D are the arguments that minimize the spatial autocorrelation (Moran's I) of the residuals

$$r(s_i) = p(s_i) - \widehat{p}_{w_0}(s_i).$$

The optimal kernel width w_p for each pattern is the value which minimizes the Moran's I in the residuals over all spots in the sample. Subsequently, the optimal outlier threshold τ_0 minimizes spatial autocorrelation of the residuals $r(s_i)$ over the spots contained in the resulting region of pattern influence. If a spot is influenced by two or more patterns, these patterns are said to be interacting in such a spot. For each pattern pair of interest, the set of all such spots is defined as their interacting region.

Statistical test to identify genes associated with pattern interactions

For a given pair of patterns p_1 and p_2 with a substantial regions of exclusive pattern influence and pattern interaction, we define three subregions characterized by

- The spots with p_1 influence and no p_2 influence.
- The spots with p_2 influence with no p_1 influence.
- The spots with overlapping influence from both p_1 and p_2 .

The elements from each row of \hat{R} corresponding to the subregions described above denote the CoGAPS residuals in the respective subregions. For each gene (row) i, we perform a non-parametric Kruskal-Wallis test⁴⁵ for stochastic dominance of the CoGAPS residuals in at least one of the three subregions, with a posthoc Dunn's test 46 to ascertain the relative dominance between the respective subregions. Of particular interest to us are the genes which have statistically significantly higher CoGAPS residuals (FDR 0.05) in the interacting region relative to the other two subregions as well as genes which exhibit statistically significantly higher CoGAPS residuals exclusively in the interacting region compared to at least one of the two other subregions.

Multi-resolution CoGAPS analysis

The ST genes by spot counts data for each sample was filtered to remove genes and spots with no or constant signal and then log₂ normalized. The final matrix size of the input data matrix \mathbf{D} are noted in the table below. The element D_{ii} represents the expression of the i-th gene in the j-th spot. The CoGAPS (version 3.5.8)³⁷ algorithm was run using the filtered and normalized counts data as input. Additionally, default CoGAPS parameters were used except for nlterations = 50,000, sparseOptimization = TRUE, distributed = single-cell, and nSets = 4. CoGAPS factorization results in two lower-dimensional matrices: an amplitude matrix (A) containing gene weights and a pattern matrix (P) containing corresponding spot weights estimated for a pre-specified number of latent features (nPatterns). On each of the input datasets, the algorithm was tested for a range of nPatterns.

nPattern values and number of learned patterns for different CoGAPS runs. The values shown in boldface are used in further analysis.

Sample	# genes	# spots	numPatterns (Learned Patterns)
PDAC metastatic lymph node	18418	1351	5(5), 8(10) , 15(21)
PanIN	16,954	1,872	5(5), 10(10)
Invasive breast ductal carcinoma	24228	4898	5(5) , 10(9), 15(14), 20(16)
HCC	20423	3006	5(4), 10(7), 15(9) , 20(10), 30(18)

The pattern weights for each spot were plotted over the tissue to show association between a pattern and a tissue region. In high-Res Breast cancer analysis, genes were assigned to the pattern they were most strongly associated with using the patternMarker function in CoGAPS (version) in R (version). The genes for each pattern were submitted to the Molecular Signatures Database and searched within the BIOCARTA, KEGG, and HALLMARK pathways. 27-29 Pathways were considered significant if FDR < 0.05.



Scatterpie visualizations

We use the A and P matrices in the CoGAPS result to represent each Visium spot as a combination of overlapping latent patterns. To this end, we calculate the fractional gene expression FSE_{kj} in pattern k at spot j as

$$spotFE_{kj} = \frac{P_{kj} \sum_{i} A_{ik}}{\sum_{k} (P_{kj} \sum_{i} A_{ik})},$$

where i is the gene index. We use the 'vizAllTopics' function from the 'STdeconvolve' package 17 to visualize each spot as a pie chart showing the fractional gene expression in each pattern.

ProjectR analysis with matched single-cell RNAseq data

For the HCC sample in Figure 6, we have matched single-cell RNAseq data from the same patient. This scRNAseq data was preprocessed using the 'sctransform' package, 47 a normalization and variance stabilization method based on regularized negative binomial regression method, available in Seurat⁴² package in R. The transfer learning method, ProjectR, was used to project the spatial patterns from the HCC sample onto matched scRNAseq data from the same patient. Although the Visium data for CoGAPS and singlecell datasets use different normalization methods, our previous studies have shown that projectR can identify related cellular attributes across various data types and modalities in spite of batch effects. 24 The R package projectR (version 1.6.0) was used to project the A matrix of the CoGAPS result into the target dataset. The CoGAPS result object and the counts data from the matched scRNAseg dataset were used as input where FULL = TRUE. Each individual cell in the scRNAseg dataset is associated with the pattern with the highest projection. We limit the pattern association to the dominant patterns in the spatial data, namely Patterns 1,2, and 8.

Gene Set Enrichment Analysis using MsigDB

For each gene list query corresponding to SpaceMarkers for pairs of patterns, we compute their overlaps with gene sets belonging to the HALLMARK, BIOCARTA and KEGG pathways in MsigDB, 27-29 and report statistically significant overlaps (FDR < 0.05).